Journal of Inorganic Biochemistry 201 (2019) 110824

Contents lists available at ScienceDirect

Journal of Inorganic Biochemistry

journal homepage: www.elsevier.com/locate/jinorgbio

# Replacement of the heme axial lysine as a test of conformational adaptability in the truncated hemoglobin THB1

Dillon B. Nye, Eric A. Johnson, Melissa H. Mai, Juliette T.J. Lecomte*

*T.C. Jenkins Department of Biophysics, Johns Hopkins University, 3400 North Charles Street, Baltimore, MD 21218, USA*

ARTICLE INFO

*Keywords:*
2-on-2 hemoglobin
TrHb1
Distal ligand
Paramagnetic NMR
pH titration

ABSTRACT

Amino acid replacement is a useful strategy to assess the roles of axial heme ligands in the function of native heme proteins. THB1, the protein product of the *Chlamydomonas reinhardtii THB1* gene, is a group 1 truncated hemoglobin that uses a lysine residue in the E helix (Lys53, at position E10 by reference to myoglobin) as an iron ligand at neutral pH. Phylogenetic evidence shows that many homologous proteins have a histidine, methionine or arginine at the same position. In THB1, these amino acids would each be expected to convey distinct reactive properties if replacing the native lysine as an axial ligand. To explore the ability of the group 1 truncated Hb fold to support alternative ligation schemes and distal pocket conformations, the properties of the THB1 variants K53A as a control, K53H, K53M, and K53R were investigated by electronic absorption, EPR, and NMR spectroscopies. We found that His53 is capable of heme ligation in both the Fe(III) and Fe(II) states, that Met53 can coordinate only in the Fe(II) state, and that Arg53 stabilizes a hydroxide ligand in the Fe(III) state. The data illustrate that the group 1 truncated Hb fold can tolerate diverse rearrangement of the heme environment and has a strong tendency to use two protein side chains as iron ligands despite accompanying structural perturbations. Access to various redox pairs and different responses to pH make this protein an excellent test case for energetic and dynamic studies of heme ligation.

## 1. Introduction

Among the many characteristics that condition the chemical reactivity of a heme protein, the axial ligands to the iron are of singular importance [1]. Besides generally contributing to thermodynamic stability through a coordination bond, they restrict the conformational space accessible to the polypeptide, affect the reduction potential of the iron and its solvent accessibility, dictate the distortions and electronic distribution of the porphyrin ring, and modulate reaction kinetics. Heme proteins belonging to different superfamilies are therefore seen to utilize different axial ligand sets, with the protein moiety controlling the number (0, 1, or 2) and identity of the ligands as function is performed. Chemically competent residues for ligation are many: histidine (which is most frequently observed), cysteine, methionine, tyrosine, occasionally lysine, and rarely asparagine, glutamine, and arginine. Any of these residues, when used as a ligand, will impose unique properties on the holoprotein. Deviations from the wild-type set, either by mutation or by an extreme change of conditions, can have disastrous consequences. The protein features that establish coordination schemes are therefore critical to designing artificial heme proteins and understanding the mechanistic aspects of natural ones.

Given the typically large number of potential heme ligands in any one protein sequence, a key factor is the formation, at least in the folded holoprotein state, of a heme cavity providing numerous stabilizing contacts and a proper degree of flexibility to control the coordination of specific residues [2,3]. In these respects, group 1 truncated hemoglobins (Hbs) stand out. They are small proteins forming a separate lineage of the Hb superfamily, distantly related to the lineage of animal Hbs, and endowed with chemical roles other than reversible binding of dioxygen [4,5]. Like the familiar Hbs, group 1 truncated Hbs use a “proximal” histidine as a ligand to the iron, but some also coordinate the iron with a “distal” histidine or lysine at neutral pH, forming endogenous, hexacoordinate His/His [6,7] or His/Lys [8,9] complexes. These proteins have the plasticity required for structural rearrangement upon binding exogenous ligands [10]. However, not all TrHbs that contain a distal histidine or lysine populate stable His/His or His/Lys states. Also, at the position aligned to these distal His and Lys, a number of group 1 truncated Hb sequences have methionine or arginine, residues mentioned above in the list of potential ligands. Thus, investigation of group 1 truncated Hbs opens the question of how to predict the heme ligand set, i.e., how the protein scaffold dictates endogenous hexacoordination.

* Corresponding author.
*E-mail address:* lecomte_jtj@jhu.edu (J.T.J. Lecomte).

https://doi.org/10.1016/j.jinorgbio.2019.110824
Received 6 August 2019; Received in revised form 3 September 2019; Accepted 3 September 2019
Available online 04 September 2019
0162-0134/ © 2019 Elsevier Inc. All rights reserved.

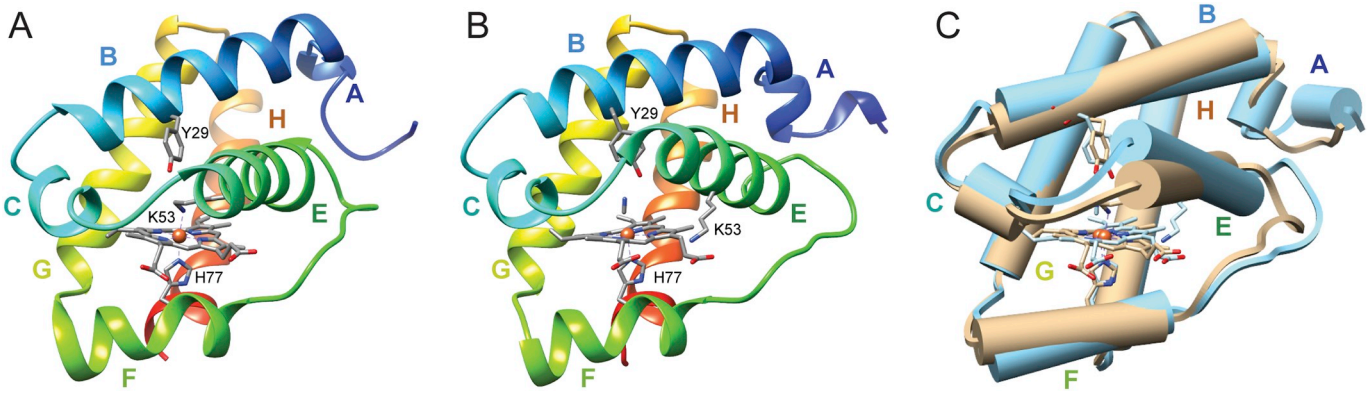


**Fig. 1.** The structure of Fe(III) WT THB1 (**A**) without added exogenous ligand showing the His/Lys coordination (PDB entry 4XDI) and (**B**) with bound cyanide (cyanomet THB1) showing the His/CN coordination (PDB entry 6CII). (**C**) shows the superposition of the two structures (4XDI, tan; 6CII, cyan). Structural rearrangement is apparent in the loops preceding and following the E helix as well as the orientation of the E helix. Helices are labeled with myoglobin nomenclature. (For interpretation of the references to color in this figure legend, the reader is referred to the web version of this article.)

THB1 is one of several group 1 truncated Hbs found in *Chlamydomonas reinhardtii*. Along with THB2 and THB4 [9], THB1 exhibits native His/Lys heme ligation [8], which is rare not only in the Hb family but also in heme proteins in general. The His/Lys scheme of THB1 dominates in both the Fe(III) and the Fe(II) states at physiological pH and becomes increasingly compromised as the pH is lowered [8]. Whereas highly acidic conditions are required to protonate the proximal histidine, the distal lysine (Lys53, or E10 following the helical nomenclature of myoglobin) is readily displaced by acidification or by addition of a high-affinity exogenous ligand, such as CO for Fe(II) or $CN^-$ for Fe(III).

Distal ligand switching is accompanied by a structural change illustrated by two X-ray structures, that of THB1 in the Fe(III) His/Lys state (Protein Data Bank (PDB) entry 4XDI, [11]) and THB1 in the Fe(III) His/CN (cyanomet) state (PDB entry 6CII, J.M. Martinez et al., manuscript in preparation) (Fig. 1). On cyanide binding, several hydrophobic groups in contact with the heme retain the same relative positions (Fig. 2). In contrast, Lys53 (E10) is displaced toward solvent as Gln50 (E7), Gln54 (E11), and Tyr29 (B10) are introduced into the heme cavity. The region most affected by Lys53 relocation is on the side of the heme 1-$CH_3$ and the 8-$CH_3$, manifesting a rearrangement of Phe57 (E15) and Tyr68 among others. The structural changes suggest that the THB1 scaffold is inherently flexible and may be able to accommodate different endogenous distal ligands.

In the present work, we explored the tolerance of the THB1 fold for different occupants at the distal position and began the analysis of the factors that regulate heme ligation. The wild-type (WT) Lys53 (E10) of THB1 was replaced to generate a series of variants. These variants exhibit at position E10 the most common residues found by multiple sequence alignments of known group 1 truncated Hbs. We focused on ligation schemes and pH response using electronic absorption, EPR, and NMR spectroscopies. Along with extensive NMR data, the two X-ray structures of WT THB1 provide a reference against which to assess the properties of E10 variants. We show that THB1 is an apt model system for the study of the interplay between protein structure and heme coordination and we lay the groundwork for detailed thermodynamic and dynamic characterization of ligand switching.

## 2. Experimental section

### 2.1. Protein preparation

The K53H, K53M, and K53R mutations were introduced into a pJExpress414 plasmid containing the *THB1* gene using the Q5 Site-Directed Mutagenesis Kit (New England Biolabs, Ipswich, MA) and primers from Integrated DNA Technologies (Coralville, IA). THB1 variants were expressed in *Escherichia coli* BL21 cells using the protocol described for the WT and K53A proteins [8]. Following overexpression and cell lysis by sonication, variant THB1 apoproteins were purified from inclusion bodies using urea solubilization and passage through a Sephadex G-50 size exclusion column equilibrated with TE buffer (50 mM Tris pH 8.0, 1 mM ethylene-diaminetetraacetic acid trisodum salt). Benzonase (MilliporeSigma, Burlington, MA) was included during cell lysis to digest contaminating DNA. Purified apoproteins were converted to holoproteins by titration with porcine hemin (Sigma, St

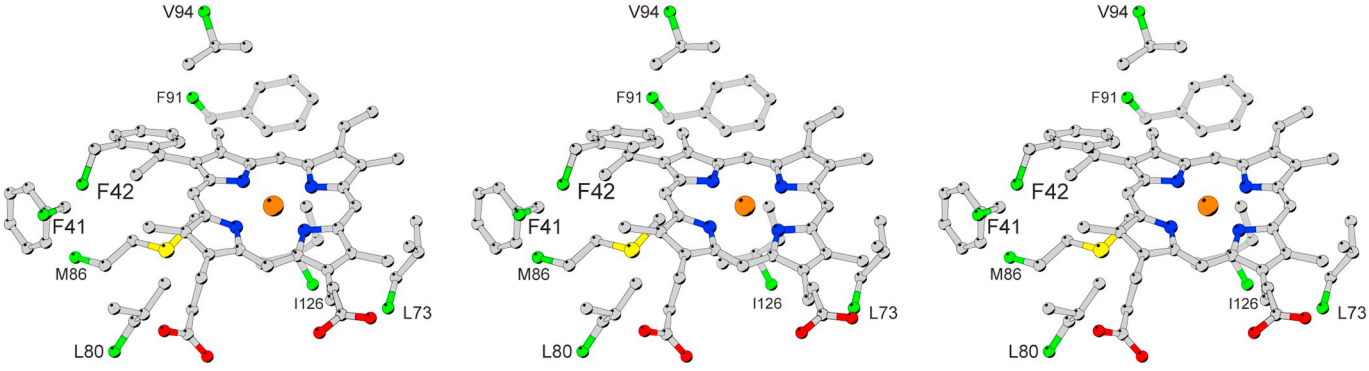


**Fig. 2.** Stereo triptych showing the residues that maintain the same position with respect to the heme group when Lys53 is replaced by cyanide. For stereo viewing, the convergent pair is on the left and the divergent pair is on the right. The structure of the His/Lys complex (PDB entry 4XDI) was used. Phe41, Phe42, Leu80 and Met86 are near the 4-vinyl and the 5-$CH_3$; Phe91, Val94, and Ile126 are near the 3-$CH_3$ and 2-vinyl; and Leu73 is near the 1-$CH_3$. The axial Lys53 (above the heme plane) and His77 (below the heme plane) are not included for clarity. The $C^\alpha$ atoms are colored in green. (For interpretation of the references to color in this figure legend, the reader is referred to the web version of this article.)

Louis, MO) dissolved in 0.1 M NaOH. This step was followed by passage through a diethylaminoethanol-Sepharose column. Purity was assessed with sodium dodecyl sulfate polyacrylamide gel electrophoresis and mass spectrometry data (Acquity/Xevo-G2 Ultra Performance Liquid Chromatography–Mass Spectrometry, Waters, Milford MA). Purified proteins were exchanged into storage buffer (5 mM sodium phosphate pH 7.5), lyophilized and stored at −20 °C. Typical yields were ~25 mg/L (K53R THB1) and ~100 mg/L (K53H, K53M, and K53A THB1s). Uniformly $^{15}$N labeled K53H THB1 and K53M THB1, and uniformly $^{13}$C, $^{15}$N labeled K53R THB1, were prepared in the same fashion from cells grown in M9 medium containing $^{15}NH_4Cl$ or $^{15}NH_4Cl$ and $^{13}$C-glucose (Cambridge Isotope Labs, Tewksbury, MA) instead of Luria-Bertani medium. Extinction coefficients were determined on a per-heme basis using the pyridine hemochromogen method [12]. Values at pH 7.4 for Fe(III) THB1 variants are as follows: K53A THB1, $\varepsilon^{406} = 130\ mM^{-1}\ cm^{-1}$; K53M THB1, $\varepsilon^{407} = 163\ mM^{-1}\ cm^{-1}$; K53H THB1, $\varepsilon^{411} = 112\ mM^{-1}\ cm^{-1}$; K53R THB1, $\varepsilon^{411} = 110\ mM^{-1}\ cm^{-1}$ with a ~5% error according to triplicate measurements. Cyanomet complexes were obtained by adding an excess of KCN to buffered samples of Fe(III) K53X THB1.

### 2.2. Electronic absorption spectroscopy

Electronic absorption spectra were collected at room temperature with a Varian Cary-50 spectrophotometer. Typical protein concentrations were 10–15 μM. For Fe(III) samples, spectra were collected from 800 to 260 nm in steps of 1 nm using a 100-ms averaging time. Fe(II) spectra were acquired from 800 to 350 nm every 1 min following the addition of 2 mM dithionite (DT, Sigma) until a stable reduced species was observed, typically within 5 min.

### 2.3. EPR spectroscopy

X-band continuous wave EPR spectra were acquired using a Bruker EMX spectrometer with a microwave frequency of 9.41 GHz, a power level of 13 mW and modulation amplitude of 10 G. Sample temperature was maintained at 10 K during acquisition using a liquid helium cryostat. THB1 variants (1 mM THB1, 10 mM sodium phosphate pH 8.0 and 0% or 10% v/v glycerol) were prepared in 5 mm outer-diameter quartz EPR tubes and frozen by gentle submersion into liquid nitrogen. Data were processed with the MatLab toolbox EasySpin 5.2.21 [13].

### 2.4. NMR spectroscopy

NMR spectra were acquired using a Bruker Avance-600 or Bruker Avance II-600, each equipped with a triple resonance inverse cryoprobe, or a Varian Inova 800 MHz spectrometer equipped with a triple resonance inverse room-temperature probe. Some data were also acquired on a Bruker Avance III-400 equipped with a triple resonance inverse room-temperature probe. $^1$H chemical shifts were referenced against the $^1H_2O$ signal (4.76 ppm) and $^{15}$N chemical shifts were referenced indirectly through the Ξ ratio [14]. Unless otherwise noted, data were collected at 25 °C in aqueous buffer. Fe(II) samples were prepared in a micro-oxic atmosphere using deoxygenated buffer and DT; the plunger of the Shigemi NMR tube and Parafilm M protected the protein from oxidation. 1-D data were analyzed using TopSpin 4.0.6 (Bruker) and 2- or 3-D data were processed using NMRPipe [15] and analyzed with Sparky [16]. Non-uniformly sampled spectra were reconstructed using the NESTA-NMR software package [17] implemented on the NMRbox virtual machine [18].

Heme $^1$H assignments were made at 600 MHz with a standard suite of $^1$H–$^1$H experiments [7] including nuclear Overhauser spectroscopy (NOESY) (with $t_1$ noise reduction [19] as helpful, $\tau_{mix}$ = 80–110 ms), double-quantum-filtered correlated spectroscopy (DQF-COSY), total correlation spectroscopy (TOCSY) ($\tau_{mix}$ = 45 ms) and, for paramagnetic species, water elimination Fourier transform (WEFT) NOESY [20] data (typical $\tau_{recycle}$ = 100 ms, $\tau_{recovery}$ = 150 ms, $\tau_{mix}$ = 40 ms). Samples were Fe(II) K53M THB1 (2.1 mM, 100 mM sodium phosphate $pH_*$ 7.2, 6 mM DT), Fe(III) K53H THB1 (1.3 mM, 20 mM sodium phosphate pH* 7.3), and Fe(III) K53R THB1 (1.3 mM, 20 mM sodium phosphate pH* 7.9) in 99% $^2H_2O$ at 25 °C. $^1$H longitudinal relaxation time ($T_1$) values for resolved signals in K53H and K53R THB1s were measured with a simple inversion-recovery sequence. Homonuclear spectra also enabled assignment of protein residues in the heme pocket by reconciling NOESY data with the THB1 X-ray structure (PDB entry 4XDI [11]).

Backbone amide $^1$H and $^{15}$N and select side chain $^1$H assignments were made at 800 MHz in Fe(II) K53M THB1 (2.5 mM, 130 mM potassium/sodium phosphate pH* 7.0, 10% $^2H_2O$, 6 mM DT) and Fe(III) K53H THB1 (1.7 mM, 50 mM potassium phosphate pH* 7.1, 10% $^2H_2O$). Assignments were achieved with $^1$H–$^{15}$N heteronuclear single-quantum correlation (HSQC), $^1$H-$^{15}$N-$^1$H NOESY-HSQC ($\tau_{mix}$ = 75 ms) and $^1$H-$^{15}$N-$^1$H TOCSY-HSQC ($\tau_{mix}$ = 45 ms) experiments and comparison to published chemical shifts for Fe(III) (Biological Magnetic Resonance Bank (BMRB) entry 26885) and Fe(II) THB1 (BMRB entry 26886). Backbone $^1H^N$, $^{15}$N, $^{13}C^\alpha$, $^{13}C^\beta$ and $^{13}C'$ assignments were made in Fe(III) K53R THB1 (1.8 mM, 20 mM sodium phosphate pH* 7.5, 5% $^2H_2O$) at 600 MHz. A suite of 3D experiments including HNCO, CBCA(CO)NH, HNCACB, HBHA(CO)NH [21], and H(CCO)NH and (H)C(CO)NH-TOCSY [22] was acquired using a Poisson-Gap sampling schedule [23] (15% sampling) in both indirect dimensions. The backbone information was completed with $^1$H-$^{15}$N-$^1$H NOESY transverse relaxation optimized spectroscopy (TROSY) data at 800 MHz ($\tau_{mix}$ = 75 ms).

Tailored $^{13}$C–$^1$H correlation experiments were acquired on K53R THB1 (1.8 mM, 20 mM sodium phosphate pH* 7.5, 5% $^2H_2O$, 25 °C, 600 MHz) to assign the aliphatic portion of the Arg53 side chain. In one experiment, two downfield protons were correlated with the directly attached $^{13}$C resonating at −1.0 ppm via $^1J_{CH}$ coupling. In the second experiment, four additional protons were correlated with the upfield $^{13}$C resonance using a $^{13}$C-TOCSY element. The pulse sequences and additional experimental details are given in Fig. S1.

Differences in backbone amide chemical shift between K53X and WT THB1 in the same oxidation state are presented as the chemical shift perturbation, $CSP = (\Delta\delta_H{}^2 + (\Delta\delta_N/10)^2)^{1/2}$ [24], where $\Delta\delta_H$ is the $^1H^N$ chemical shift of K53X THB1 minus that of WT THB1 and $\Delta\delta_N$ is the corresponding difference of $^{15}$N shifts. Differences in chemical shifts ($\Delta\delta$) between Fe(III) K53X THB1 (where X is H or R) and Fe(II) WT THB1 were used in the program Numbat along with the crystal structures of THB1 (His/Lys, PDB entry 4XDI; His/$CN^-$, PDB entry 6CII; $^1$H added with UCSF Chimera [25]). If the positions of the nuclei, relative to the heme plane and iron, are unchanged from the crystal structure and the amino acid substitution has no effect on the diamagnetic shift, $\Delta\delta$ for residues except the proximal histidine and X at E10 is the pseudocontact shift (PCS). The PCS is given by

$$\delta_{pc,i} = \frac{1}{12\pi r_i^3}\left[\Delta\chi_{ax}(3\cos^2\theta_i - 1) + \frac{3}{2}\Delta\chi_{rh}\sin^2\theta_i\cos 2\varphi_i\right]$$

in the frame of reference in which the susceptibility tensor, $\chi$, is diagonal. In this coordinate frame with the paramagnetic center at the origin, the spherical polar coordinates $r_i$, $\theta_i$ and $\varphi_i$ specify the location of the i$^{th}$ nucleus [26]. Parameters $\Delta\chi_{ax}$ and $\Delta\chi_{rh}$ are the axial and rhombic components of the tensor, respectively. Finding a tensor that accounts for all $\Delta\delta$ values validates the isostructural assumption.

### 2.5. pH titrations

Electronic absorption spectra were acquired on Fe(III) K53A, K53H, K53M and K53R THB1s over the pH range 3–13. Protein samples (~10 μM protein per heme basis, 5 mM sodium phosphate) were prepared at neutral pH and spectra were acquired as titrant (HCl for pH 3–7.5 or NaOH for pH 7.5–13) was added. The pH was measured

before and after acquisition of a spectrum and a correction for sample dilution was applied. K53A, K53M and K53R THB1 showed spectral changes in the pH range 4–11 indicative of a change in heme ligation. In each case, the titration event was incompletely resolved from either an acid (K53R THB1) or a base (K53A and K53M THB1s) process. To extract apparent p$K_a$ values, singular value decomposition was applied to titration data sets [27] as described previously [8]. The two or three most significant abstract vectors were globally fit to one or a sum of two Henderson-Hasselbalch equations including Hill coefficients, yielding one or two apparent p$K_a$ values. The analysis was carried out either with Mathematica 12 or MatLab R2019a.

Electronic absorption spectra of Fe(II) K53H THB1 were recorded at several pH values to assess iron coordination in the reduced state. Protein concentration (~10 μM) was determined by measurement of the absorbance at the Soret maximum in the Fe(III) state at desired pH values between pH 5.0 and pH 6.0 (100 mM 2-(*N*-morpholino)ethanesulfonic acid) and between pH 6.0 and 8.0 (100 mM potassium phosphate). The sample was then reduced by addition of a known volume of concentrated DT. Spectra were collected as a function of time over a few minutes. Equilibrated reduced state spectra were extracted from the time course. Below pH 5, the samples were unstable. Absence of baselines and isosbestic points prevented the determination of an apparent p$K_a$ for the transition.

### 2.6. Binding of ammonia to Fe(III) K53M THB1

A 3 M stock solution of $NH_4Cl$ in 100 mM potassium phosphate, pH 7.0, was serially diluted to a concentration of ~5 mM in 100 mM potassium phosphate, pH 7.0. Lyophilized Fe(III) K53M THB1 was dissolved in 100 mM potassium phosphate, pH 7.0, to a final stock concentration of 750 μM. This solution was added to each $NH_4Cl$ solution to reach a final protein concentration of 10 μM. The pH was measured and re-adjusted to 7.0, if necessary, and the spectrum of the mixture was collected until the absorbance remained stable. The pH of the sample was measured again after data collection. To analyze the titration results, a singular value decomposition approach was applied, yielding two significant abstract vectors. A single-site quadratic equation was fit to the data with correction for the dissociation of $NH_4^+$ (p$K_a$ = 9.25). The analysis was carried out with MatLab R2019a.

### 2.7. Protein sequence analysis

The amino acid sequence of THB1 was used in a Basic Local Alignment Search Tool (BLAST) search [28] (May 19, 2019 with expect threshold of 1e−6, 95% redundancy cut-off, sequence length between 100 and 150 residues, containing group 1 truncated Hb markers: Gly-Gly pair in the AB turn, Tyr at B10 and proximal His). A total of 1047 sequences were retained and aligned with Clustal from JalView [29]. Occupancy at E10 was 58 Met, 75 Arg, 344 Lys, 541 His, and a few instances of Leu, Gln, Asn, Thr, and Tyr.

## 3. Results

The first step in the distal ligation study was to generate variants of the THB1 protein in which the native lysine at position E10 (K53) was replaced with a series of substituting residues. Each of the resulting K53X THB1 proteins was readily prepared and bound heme in both the Fe(III) and Fe(II) states. However, it is known that the replacement of E10 in some group 1 truncated Hbs can cause a repositioning of the cofactor within the fold [30]. To determine if the K53X proteins are able to adopt a conformation closely resembling the WT protein, the $^1$H NMR spectrum of the cyanide adduct of the Fe(III) state was inspected. Spectroscopically, cyanide binding to a ferric globin results in the formation of a paramagnetic low-spin cyanomet complex and the appearance of distinctive hyperfine shifted resonances readily detected in the 1D $^1$H spectrum [31]. Fig. 3 illustrates the common spectral features between the variants and WT THB1. Of note is the signal from the phenolic proton of Tyr29 (B10) at ~ 26 ppm, which reports on direct interaction with the bound cyanide [32]. Small chemical shift differences are observed, but overall the data support that, in each variant, residue 53 is displaced from the binding site to accommodate Tyr29, Gln50 and Gln54. Having established the integrity of the holoproteins when a strong ligand is present, we proceed with the description of the E10 variants in the absence of exogenous ligand.

### 3.1. K53A THB1

#### 3.1.1. Heme coordination in K53A THB1

K53A THB1 was used in prior work toward the identification of the WT distal ligand [8]. The results are summarized and complemented here. At neutral pH, the electronic absorption spectrum of Fe(III) K53A THB1 exhibits a charge transfer band at ~630 nm (Fig. 4A). In addition, the $^1$H NMR spectrum contains hyperfine-shifted signals down to 80 ppm and none detectable in the −10 to −40 ppm region, which led us to propose that a distal $H_2O$ coordinates the iron [8]. Raising the pH causes changes in the absorption spectrum (Fig. 5A,B) that are consistent with deprotonation of the bound $H_2O$. This “aquomet to hydroxymet” transition occurs with a relatively high apparent p$K_a$ of ~9.6 (Fig. S2, Table S1).

To characterize the spin state of Fe(III) K53A THB1 as a reference for other variants, the low-temperature EPR spectrum was acquired at pH 8.0. Two features ($g_\perp$ = 5.89, $g_\parallel$ = 1.97, Fig. 6A) are observed in agreement with a high-spin ($S$ = 5/2) iron complex. Upon reduction to the Fe(II) state, the NMR and electronic absorption spectra of Fe(II) K53A THB1 are characteristic of a pentacoordinate heme at neutral pH. Heme coordination in K53A THB1 is thus similar to that of sperm whale myoglobin, involving the proximal histidine as sole protein ligand in both oxidation states. The heme coordination features of K53A THB1 are summarized in Table 1.

### 3.2. K53M THB1

#### 3.2.1. Heme coordination in K53M THB1

Methionine is found as a native iron ligand in a number of heme proteins, most notably the ubiquitous electron transfer protein cytochrome *c* [33]. Met E10 is present in ~6% of group 1 truncated Hb sequences, and, if able to coordinate the iron, would impact exogenous ligand binding and electron transfer reactions. For Fe(III) K53M THB1, the electronic absorption (Fig. 4B) and EPR (Fig. 6B) spectra indicate a high-spin species. The extinction coefficient of the Soret band (407 nm) is relatively high (163 $mM^{-1}\,cm^{-1}$) at pH 7.4, which suggests coordination of a water molecule rather than a pentacoordinate heme [34]. In addition, no charge transfer p(S) → $d_\pi(Fe^{3+})$ transition typical of His/Met complexes is detected at ~695 nm [35]. Increasing the pH reveals a transition (Fig. 5C,D) with an apparent p$K_a$ of ~10 attributed to the ionization of the bound water molecule to hydroxide (Fig. S2, Table S1). A further transition involving tyrosine ionization occurs with an apparent p$K_a$ of ~11.6.

Fe(II) K53M THB1 displays resolved α and β bands at 560 nm and 530 nm (Fig. 4B). These are signatures of a heme iron coordinated by two strong-field axial ligands and correspond well to the α and β bands of ferrocytochrome *c* (550 nm and 520 nm) [36], after accounting for a 10-nm hypsochromic shift caused by vinyl saturation in *c* heme [12]. The $^1$H NMR spectrum of Fe(II) K53M THB1 (Fig. 7A) has sharp signals confined within −3 ppm and 12 ppm, in agreement with a diamagnetic complex, presumably of the His/Met kind. To confirm that Met53 is a heme ligand, uniformly $^{15}$N-labeled protein was investigated with NMR spectroscopy.

Two distinct forms of K53M THB1 are apparent in the $^1$H–$^{15}$N HSQC spectra (Fig. S3). A priori, these arise from slowly-exchanging forms of the holoprotein binding the heme in orientations related by a ~180° rotation about the axis defined by the α- and γ-*meso* carbons of the

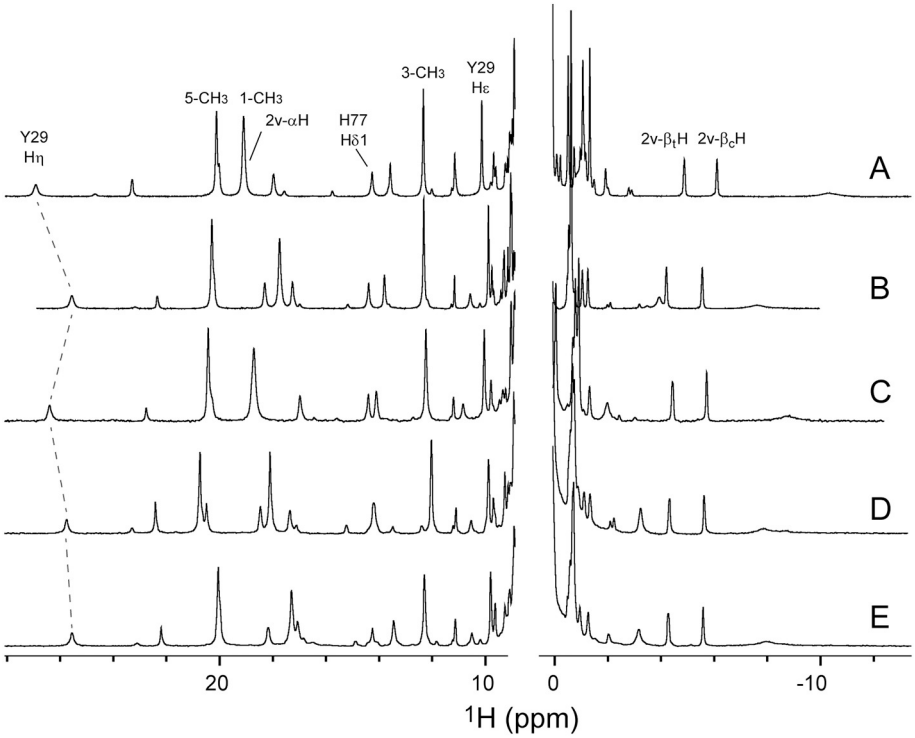


**Fig. 3.** $^{1}$H spectra of cyanomet WT and K53X THB1 in 10% $^{2}H_2O$, pH 7.6–8.0. (**A**) WT THB1 and (**B**) K53A THB1 (600 MHz); (**C**) K53R THB1; (**D**) K53H THB1; and (**E**) K53M THB1 (400 MHz).

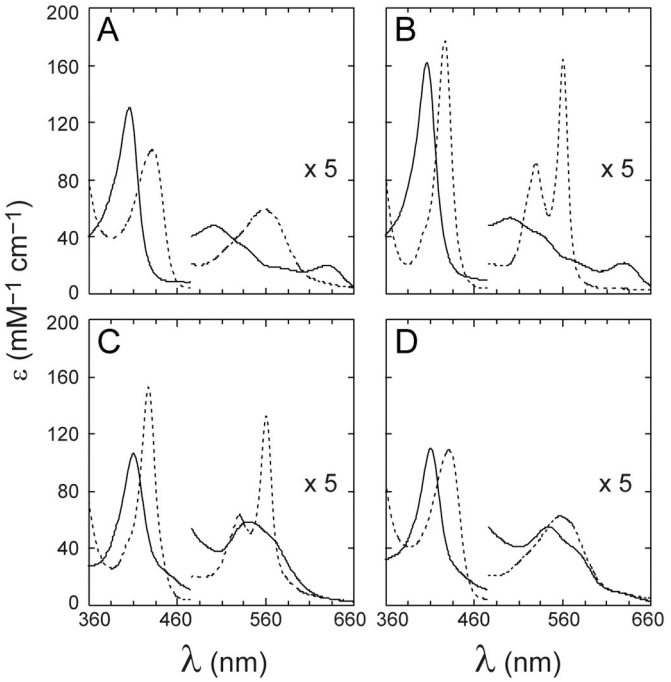


**Fig. 4.** Electronic absorption spectra of Fe(III) (solid line) and Fe(II) (dashed line) K53A (**A**), K53M (**B**), K53H (**C**) and K53R (**D**) THB1 at pH 7.5.

porphyrin (Fig. 7E) [37]. $^{15}$N-edited NOESY and TOCSY data were used for sequential assignment of backbone amide NH groups (major isomer listed in Table S2). Each Met53 $H^{N}$ was correlated with its $H^{\alpha}$, and subsequently with the resolved $H^{\beta1/\beta2}$ and $H^{\gamma1/\gamma2}$ methylene protons in the DQF-COSY data (Fig. S4). Nuclear Overhauser effects (NOEs) between these and the three-proton signals at −2.74 ppm (major isomer) or − 2.87 ppm (minor isomer) secure assignment as the Met53 $C^{\varepsilon}H_3$ group [38]. NOEs between Met53 and heme protons assigned with $^{1}$H data (Table 2, Table S3) further confirms the location of the side chain in the heme cavity and heme orientational disorder. We note that the minor isomer is populated slowly after reduction of the ferric state (Fig. S5B) and that its lines are sharper. The reason for the differential linewidth is not clear, though likely related to a dynamic process modulated by the immediate environment of the heme group. In all, the diamagnetic properties of Fe(II) K53M THB1, strong ring current shift experienced by Met53, and heme–Met53 NOEs support that Met53 is able to substitute for Lys53 as distal heme ligand in Fe(II) THB1. The heme coordination features of K53M THB1 are summarized in Table 1.

### 3.2.2. *Structural properties of Fe(II) K53M THB1*

NOEs between heme and protein (Fig. S5A) show that the major Fe(II) K53M THB1 isomer houses the heme in the same orientation as WT THB1. As a consequence, the Fe(II) state chemical shifts can be directly compared. Combined differences in amide $^{1}$H and $^{15}$N shifts (CSP) are shown in Fig. 8B. Significant perturbations (> 1 standard deviation from mean) are localized to a region stretching from the end of the C helix into the EF loop (residues 39–70). In contrast, amide shifts in the G and H helices (residues 87–128) are nearly insensitive to the K53M replacement. Magnetization transfer to water in the $^{15}$N-edited NOESY data of Fe(II) K53M THB1 is observed for the A helix, disordered C-terminus, and EF loop, as expected of structurally fluctuating regions (Fig. S6). Additionally, transfer is detected at the beginning of the E helix, which suggests this region is prone to fraying. These observations present the C–EF region as a displaceable element of structure.

NOEs to the resolved $C^{\varepsilon}H_3$ in Fe(II) K53M THB1 report on the distal pocket geometry (Fig. S7). Weak dipolar contacts to the heme α-meso-H, β-meso-H, 1-$CH_3$, and 3-$CH_3$ demonstrate an orientation of the methyl group toward pyrroles B and C. The rather large distance span for these $C^{\varepsilon}H_3$-centered NOEs suggests that the sulfur undergoes fluxion [39], switching between *R* and *S* isomers. In WT THB1, the ring of Tyr29 (B10) is shifted upfield and has NOEs to Lys53; in K53M THB1, Tyr29 has closely similar chemical shifts and is in dipolar contact with Met53. In neither protein is the tyrosine ring positioned to make a $O^{\eta}H$ hydrogen bond to the ligating $N^{\zeta}$ or $S^{\delta}$, unlike in cytochrome *c* [40].

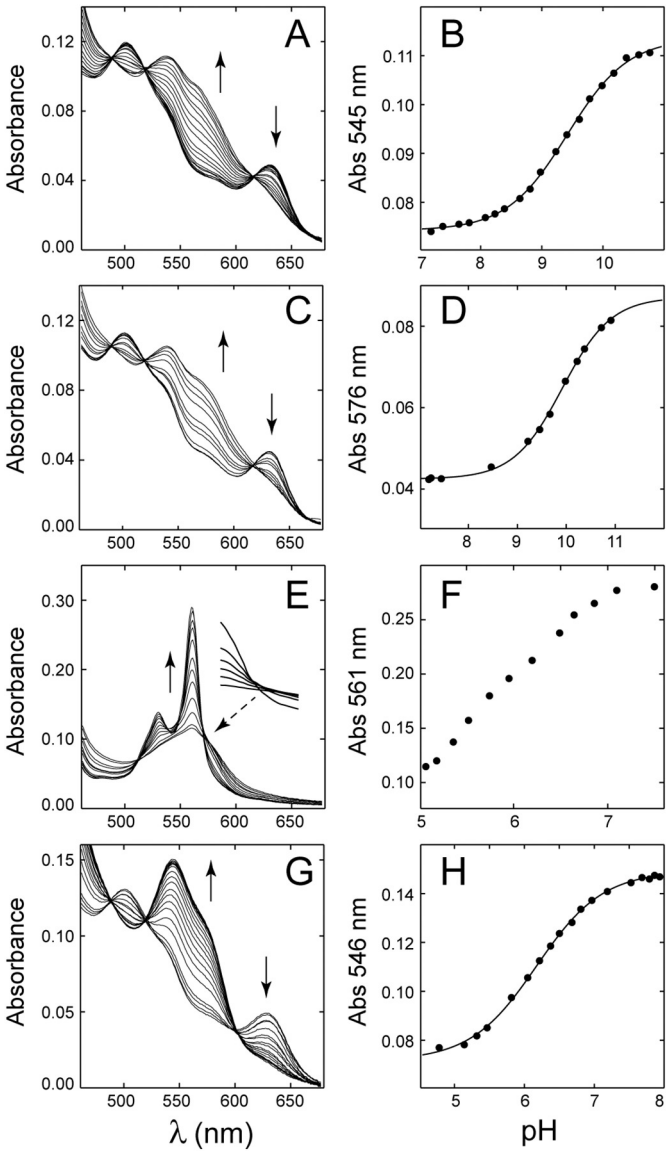


**Fig. 5.** UV–vis pH titrations of (**A**, **B**) Fe(III) K53A, apparent p$K_a$ 9.61 ± 0.02; (**C**, **D**) Fe(III) K53M, apparent p$K_a$ 10.04 ± 0.03; (**E**, **F**) Fe(II) K53H, apparent p$K_a$ ~ 6; and (**G**, **H**) Fe(III) K53R, apparent p$K_a$ 6.18 ± 0.01. In the electronic absorption spectra, solid arrows denote the spectral changes as the pH is raised. Note the different pH scales in the right panels. The solid line was calculated with the global fit parameters. The inset in Panel E uses 6 pH values to show the imperfect isosbestic crossing at 572 nm for Fe(II) K53H THB1. Additional information is presented in Table S1 and Fig. S2.

NOEs involving Tyr29 (B10), Ile32, Phe42, Phe91, Val94 and Ile126 reflect a conserved arrangement of the distal pocket in the reduced state of the K53M variant (Fig. 2).

### 3.2.3. Binding of ammonia by Fe(III) K53M THB1

According to the electronic absorption data, Met53 is displaced by a water molecule when the heme is oxidized to the Fe(III) state. However, the NMR spectrum of the His/$OH_2$ states differs from those of WT and K53A THB1 in that the high-spin heme methyl resonances are barely detectable (not shown). Assuming that WT and K53A THB1 behave like aquomet *Paramecium caudatum* group 1 truncated Hb (PDB entry 1DLW [41]), which has the B10/E7/E11 network of interactions as in cyanomet THB1 and Lys E10 outside of the heme pocket, the aquomet spectral differences observed in Fe(III) K53M THB1 suggest altered

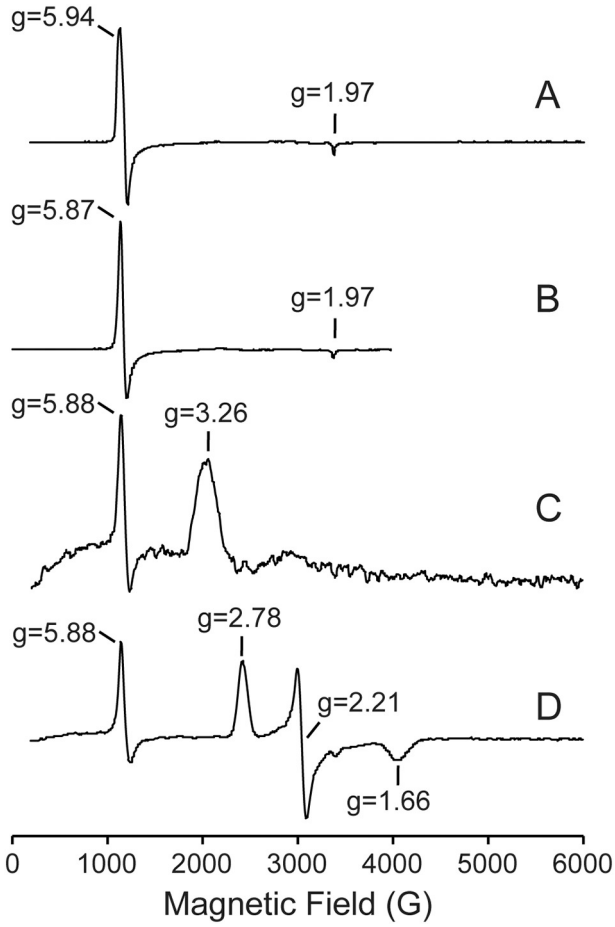


**Fig. 6.** The EPR spectra of Fe(III) (**A**) K53A, (**B**) K53M, (**C**) K53H and (**D**) K53R THB1 acquired at pH 8.0 and 10 K. Data collected with a microwave frequency of 9.41 GHz, a power level of 13 mW and modulation amplitude of 10 G.

**Table 1**
Absorption maxima of WT and E10 variants of THB1.

| THB1 | Distal ligand | pH | $S$[a] | Fe(III) $\lambda_{max}$ (nm) | Fe(II) $\lambda_{max}$ (nm) |
|---|---|---|---|---|---|
| WT | Lys53 | 7.1 | 0 | | 426, 529, 559 |
| | $H_2O$ | 4.8 | 5/2 | 408, 503, 630 | |
| | Lys53 | 7.1 | 1/2 | 410, 536, 568 (sh) | |
| K53A | – | 7.5 | 2 | | 431, 558 |
| | $H_2O$ | 7.5 | 5/2 | 405, 500, 630 | |
| | $OH^-$ | 10.8 | 5/2, 1/2 | 410, 538, 570 (sh), 627 (sh) | |
| K53M | M53 | 7.5[b] | 0 | | 427, 530, 560 |
| | $H_2O$ | 7.5 | 5/2 | 406, 500, 628 | |
| | $OH^-$ | 10.9 | 5/2, 1/2 | 409, 540, 575 (sh), 640 (sh) | |
| K53H | H53 | 7.5 | 0, 2 | | 427, 530, 560 |
| | H53 | 7.5[b] | 1/2 | 410, 540, 572 (sh) | |
| K53R | – | 7.5 | 2 | | 431, 556 |
| | $H_2O$ | 5.1 | 5/2 | 405, 500, 630 | |
| | $OH^-$ | 7.5 | 1/2 | 411, 545, 579 (sh), 631 (sh) | |

[a] Dominant spin state or likely mixture.
[b] Spectrum independent of pH over the range 4–8.

conformational dynamics and the possibility that Met53 remains in the heme cavity once the iron is oxidized.

In attempts to determine the fate of Met53 in the His/$OH_2$ complex, conditions were screened for the crystallization of Fe(III) K53M THB1, including those that were productive with the WT protein and

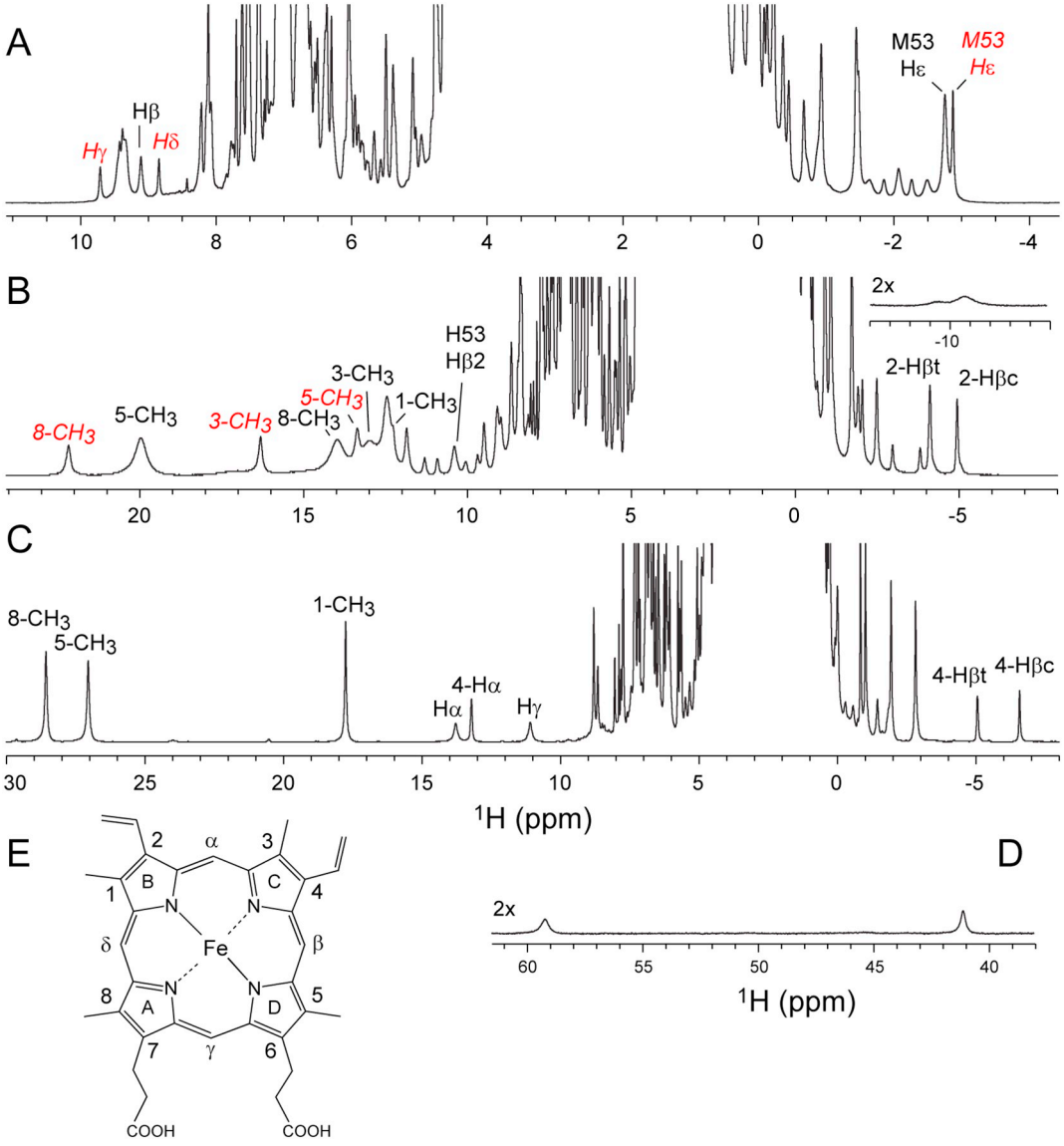


**Fig. 7.** $^{1}$H NMR spectra of Fe(II) K53M (**A**), Fe(III) K53H (**B**) and Fe(III) K53R (**C**, **D**) THB1 in $^{2}H_2O$. Assignments for selected resolved resonances are given. Assignments in red and italics are for the minor heme isomer, which is present at the level of ~40% in Fe(II) K53M THB1 and ~25% in Fe(III) K53H THB1. (**E**) The structure of heme and the nomenclature used in the text. (For interpretation of the references to color in this figure legend, the reader is referred to the web version of this article.)

contained ammonium sulfate [11]. A change of sample color to bright red was observed when that particular additive was used. Further investigation led to the conclusion that, unlike Fe(III) WT THB1, Fe(III) K53M THB1 binds ammonia. The apparent binding constant was determined with a titration at pH 7.0 (Fig. S8). After correction for the dissociation constant of the ammonium ion, the apparent association constant $K_a$ of $NH_3$ is estimated at 0.7 $mM^{-1}$.

Ammonia binding has been reported in a few heme proteins, either as the product of an enzymatic process (cytochrome *c* nitrite reductase [42]) or the result of crystallization conditions (*Rhodnius prolixus* nitrophorin 4 [43] and *Arthromyces ramosus* peroxidase [44]). In the present instance, stabilization of the His/$NH_3$ complex may be occurring as the protein retains the His/Lys conformation, Met53 mimicking the hydrophobic portion of Lys53 and ammonia its amino group.

### 3.3. K53H THB1

#### 3.3.1. Heme coordination in K53H THB1

Histidine is frequently found at position E10 in group 1 truncated Hbs. Compared to lysine, histidine has fewer degrees of freedom and its planar five-membered ring restricts the number of possible orientations it can assume within the heme pocket. Two instances of His/His coordination have been documented in WT group 1 truncated Hbs [6,7]. These proteins show that the fold can be adjusted to satisfy different constraints, but the sequences are only 42–44% identical to THB1. Within a constant protein scaffold and as the sole variation, it is not obvious that lysine and histidine are interchangeable ligands.

The electronic absorption spectrum of Fe(III) K53H THB1 (Fig. 4C) resembles that of the WT protein. As such, it suggests that His53 can indeed reach and coordinate the iron in the Fe(III) oxidation state. The low-temperature EPR spectrum (Fig. 6C) shows a minor high-spin species ($g_\perp = 5.88$, $g\|$ not detected) and a major low-spin species with a single broad feature at $g = 3.33$. This "strong $g_{max}$" signature ($g_{max} > 3$, [45]) is observed in some *bis*-histidine cytochromes and arises when the axial imidazole planes are perpendicular to each other [46]. The NMR spectrum of the same sample shows no detectable evidence for a high-spin species. In agreement with the major EPR species, the $^{1}$H chemical shift dispersion is typical of a principally low-

**Table 2**
Heme $^1$H chemical shifts and select $T_1$ values for THB1 variants.

| | Fe(II) K53M | Fe(III) K53H | | Fe(III) K53R | |
|---|---|---|---|---|---|
| | δ (ppm) | δ (ppm) | $T_1$ (ms)[a] | δ (ppm) | $T_1$ (ms)[a] |
| 1-$CH_3$ | 3.32 | 12.48 | | 17.76 | 90 |
| 3-$CH_3$ | 3.58 | 13.04 | 121 | 0.75 | |
| 5-$CH_3$ | 2.76 | 20.02 | 161 | 27.04 | 83 |
| 8-$CH_3$ | 3.40 | 14.01 | 207 | 28.56 | 87 |
| Order | | 5 > 8 ~ 3 ~ 1 | | 8 ~ 5 > 1 > 3 | |
| Average | | 14.9 | | 18.5 | |
| Span | | 7.5 | | 27.8 | |
| α-Meso | 9.32 | 2.66 | | 11.09 | 14 |
| β-Meso | 9.11 | 1.31 | | −0.29 | |
| γ-Meso | 9.35 | −1.01 | | 13.78 | 12 |
| δ-Meso | 9.44 | −0.51 | | −1.84 | |
| Order | | α > β > δ > γ | | γ > α > β > δ | |
| Average | | 0.6 | | 5.7 | |
| Span | | 3.7 | | 15.6 | |

[a] Inversion recovery spectra and fits for Fe(III) complexes are shown in Figs. S9 and S14. Labels for the heme $^1$H signals are given in Fig. 7E. Additional heme $^1$H assignments are given in Table S3.

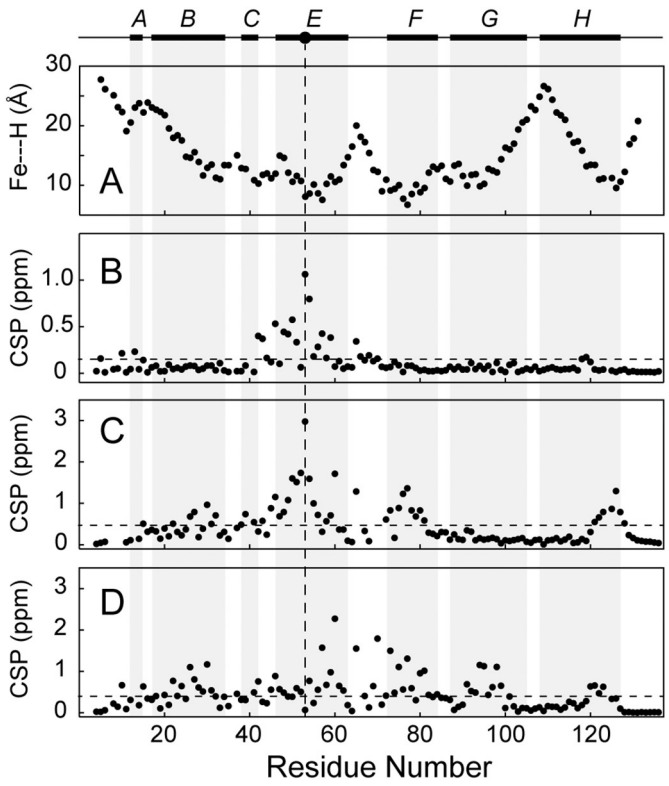


**Fig. 8.** Comparison of K53M, K53R and K53H THB1 backbone NH chemical shifts with the chemical shifts of WT THB1 in the same oxidation state. The data are presented as the combined chemical shift perturbation as calculated with $CSP = (\Delta\delta_H^2 + (\Delta\delta_N/10)^2)^{1/2}$ ppm [24]. The italicized letters at top denote the helices of the His/Lys THB1 structure (PDB entry 4XDI); the dot and vertical dashed line indicate the location of residue 53. Helices are represented in the plots as gray bars. (**A**) Distance between the iron and the amide $H^N$. (**B**) Fe(II) K53M THB1 – Fe(II) WT THB1 (BMRB entry 26886). (**C**) Fe(III) K53H THB1 – Fe(III) WT THB1 (BMRB entry 26885). (**D**) Fe(III) K53R THB1 – Fe(III) WT THB1. The horizontal dashed lines in **B–D** indicate 1 standard deviation from the mean CSP.

spin species (Fig. 7B) [47]. Assignment of the heme protons was accomplished with homonuclear data (Table 2, Table S3). Non-selective $^1$H $T_1$ values of the heme $CH_3$ groups (Fig. S9) vary between 100 ms and 200 ms, within the range of *bis*-histidine heme proteins [47]. $^{15}$N-edited NOESY and TOCSY spectra (see below) identify the $H^{\alpha}$ and $H^{\beta1/\beta2}$ signals of His53, the chemical shifts and $^1$H $T_1$ values of which (Fig. S9) situate them in close proximity to the iron in agreement with $N^{\varepsilon2}$ coordination.

The orientation of axial heme ligands determines the spin density throughout the porphyrin [48]; as a result, the heme $^1$H chemical shifts also report on geometry through contact and pseudocontact contributions to the hyperfine shift. The dispersion of the heme $CH_3$ groups in Fe(III) K53H THB1 is smaller than 10 ppm, and the order (5 > 8 ~ 3 ~ 1) is unusual among examples in which the contact contribution dominates the shifts. The nearly perpendicular arrangement of two equivalent planar ligands suggested by the EPR data is observed in the native *bis*-histidine complexes of *Synechocystis* and *Synechococcus* GlbN [49,50] and is plausible for K53H THB1 as well. Nearly perpendicular axial ligand planes minimize and level the contact contribution, which is the likely explanation for the ranking of the heme methyl signals. The heme methyl signals are sharper and more dispersed in the minor than the major isomer (Table S3). The origin of the differential linewidth is attributed to a dynamic process as for K53M THB1.

Narrow α (560 nm) and β (530 nm) bands in the Fe(II) K53H THB1 absorption spectrum (Fig. 4C) indicate that His53 ligation is maintained in the reduced state at neutral pH. Unlike the Fe(III) complex, which is unchanged as the pH is lowered to 3.6 (Fig. S2), Fe(II) K53H THB1 displays spectral changes in the neutral pH range (Fig. 5E,F). On close inspection, the spectra do not have well-defined isosbestic points (see, e.g., the inset in Fig. 5E). At pH below 5, the sample is unstable and no acid baseline could be determined. Singular value decomposition of the truncated data and global fitting returned an unrealistic low pH spectrum. Thus, although a transition is observed with a midpoint at pH ~6, reporting a precise apparent p$K_a$ associated with the optical data is not warranted. It is likely that the complex response reflects the participation of an additional species as in WT THB1 [8]. Furthermore, above pH 7.5, the $^1$H NMR spectrum of Fe(II) K53H THB1 (Fig. S10A) does not resemble a purely *bis*-histidine diamagnetic complex. Spectral changes indicative of chemical exchange on the ~μs–ms timescale are observed as the temperature is lowered (Fig. S10B–D) and below 10 °C broad features appear, similar to those of the high-spin heme in Fe(II) K53A THB1 (Fig. S10E). We conclude that His53 ligation in the THB1 scaffold is strained, resulting in a dynamic mixture of hexa- and pentacoordinate complexes at neutral pH and 25 °C. This mixture complicates the NMR spectra and a chemical shift analysis such as performed on Fe(II) K53M THB1 was not warranted. The heme coordination features of K53H THB1 are summarized in Table 1.

### 3.3.2. Structural properties of Fe(III) K53H THB1

The $^1$H–$^{15}$N HSQC spectrum of Fe(III) K53H THB1 is shown in Fig. S11; assignments of the major heme orientational isomer are listed in Table S2. Magnetization transfer to $H_2O$ is detected in the $^{15}$N-separated NOESY data for the same $H^N$ as noted in the K53M variant. Differences in amide $^1$H and $^{15}$N shifts between Fe(III) K53H and Fe(III) WT THB1 (Fig. 8C) reflect changes in the structure and in the magnetic susceptibility tensor. Not surprisingly, regions of large CSP map to shorter distances to the iron (Fig. 8A), where both factors are more likely to contribute. To explore this further, the chemical shifts of $H^N$ and select $H^{\alpha}$ of Fe(II) WT THB1 were subtracted, as a diamagnetic reference, from the corresponding shifts of Fe(III) K53H THB1 to generate a set of Δδ values. If the two structures are identical, the Δδ for residues at positions other than E10 and the proximal histidine is the pseudocontact contribution to the chemical shift (PCS). The PCS can then be used to determine the magnetic susceptibility tensor of the iron with the coordinates of the WT structure [26]. Attempts to converge on a tensor using the WT-based Δδ and structure 4XDI (lysine-bound) or 6CII (cyanide-bound) returned acceptable values for the G and H helices, which are practically not affected by exogenous ligand binding, but deviations were large in the B and E helices. This supports that the

structure undergoes some distal distortion to accommodate the non-native ligand set. On the proximal side, Ile126 and Phe91 appear to be broadened along with the 3-$CH_3$, which obscures the NOEs expected per Fig. 2. Distortions may include a displacement of the heme group, which would certainly invalidate the tensor calculation using the WT structure.

NOEs among distal pocket residues (Fig. S12) allow for a minimal structural description. The ring of Phe42 contacts His53 $H^{\beta1/\beta2}$ as well as Ile32 $C^{\gamma2}H_3$. Ile32 participates in a network of NOEs with Val94 and Phe28, which are adjacent in the structure. NOEs are detected between Tyr29 $H^{\varepsilon}$ and Arg51 $H^{N}$ and $H^{\alpha}$ protons, consistent with a relative motion of the B and E helices and a displacement of Tyr29. Phe57 $H^{\zeta}$ is in contact with Leu98, Val61 and additionally Val119, indicating a structural change necessary to provide space for His53. His77 $H^{\delta1}$ was assigned (15.6 ppm) on the basis of $^{15}N$ correlation and intraresidue NOEs, but His53 $H^{\delta1}$ was not detected, probably reflecting the absence of a hydrogen bond and penetration of solvent into the heme pocket.

### 3.4. K53R THB1

#### 3.4.1. Heme coordination in K53R THB1

In a representative set of group 1 truncated Hb sequences, arginine occupies position E10 with a frequency of ~7%. Although there is no strong expectation of heme coordination by an arginine, the role of this residue in the active site of heme proteins such as peroxidases makes the K53R protein interesting in other respects. Besides direct coordination, two extreme scenarios are conceivable, one in which the charged Arg E10 situates itself inside the heme pocket to stabilize an exogenous ligand or participate in chemistry, and another in which Arg E10 turns to solvent and interacts with the heme propionates. The electronic absorption spectra (Fig. 4D) show that in the Fe(II) state, the protein shares with K53A THB1 the characteristics of a pentacoordinate spectrum. In the Fe(III) oxidation state at neutral pH, however, the spectrum of K53R THB1 lacks the charge transfer band characteristic of high-spin complexes. This band appears when the solution pH is lowered below 7 (Fig. 5G). The apparent p$K_a$ of the transition is 6.2 (Fig. S2, Table S1) and the NMR spectrum of the low pH state is consistent with that of a water-bound complex (Fig. S13).

The low-temperature EPR spectrum of Fe(III) K53R THB1 (Fig. 6D) at pH 8.0 demonstrates a principally low-spin iron with $g_z = 2.78$, $g_y = 2.21$ and $g_x = 1.66$. A small contribution from a high-spin species is also detected. For the major species, an estimate of the rhombicity and tetragonal field parameters ($|V/\Delta| = 0.54$ and $|\Delta/\lambda| = 4.23$) places the protein at the edge of the "O" region of the truth diagram [51], suggesting that an oxygen atom is bound to the heme iron opposite the proximal histidine. A comparison of *g* values with proteins known to have an O ligand is given in Table S4, which includes one truncated Hb example (hydroxymet form of the group 2 truncated Hb from *Thermobifida fusca* [52]). The crystal field parameters are also close to those observed for the "H" region, which predicts a nitrogenous ligand. There is no compelling histidine or lysine candidate, and Arg53 itself seems unlikely because of its high p$K_a$. Possible O-ligands are Tyr29, as tyrosinate, or hydroxide, which combined with enhanced imidazolate character of His77 could give rise to the low tetragonal field parameter. The electronic absorption spectrum is markedly different from that of known His/Tyr$O^-$ Hbs [53,54], but similar to that of alkaline hydroxymet M80A cytochrome *c* [55]. Because ligation of a tyrosine would require a comparatively large structural perturbation, hydroxide ligation is the preferred working hypothesis.

The $^1H$ NMR spectrum of K53R THB1 in $^2H_2O$ at pH* 8 (Fig. 7C) displays sharp lines dispersed between 30 ppm and −10 ppm and two broad, one-proton peaks shifted far downfield at 41 ppm and 59 ppm (Fig. 7D). Homonuclear $^1H$ experiments assigned the heme resonances (Table 2), none of which corresponded to these shifted peaks. The $^1H$ $T_1$ values of the heme $CH_3$ are ~90 ms (Fig. S14) and their inverse temperature (1/T) dependence is linear (Fig. S15), two features consistent with a principally low-spin Fe(III) complex 25 °C. The heme $CH_3$ hyperfine shifts are smaller than those of hydroxymet sperm whale myoglobin or *P. aeruginosa* HasA [56], which are mixtures of $S = 1/2$ and $S = 5/2$ spin states at temperatures accessible by solution NMR spectroscopy. Hydroxymet M80A cytochrome *c* displays heme $CH_3$ shifts between 30 ppm and 10 ppm, but with $T_1$ values < 10 ms attributed to axial ligation by the weak hydroxide ligand [57]. Thus, the NMR spectral properties of Fe(III) K53R THB1 are only partially like those of documented His/$OH^-$ complexes.

The ordering of the heme methyl proton chemical shifts in heme proteins with His/cyanide ligands has been used to infer the orientation of the proximal histidine with respect to the heme plane [58]. In cyanomet THB1, the 5 ~ 1 > 3 > 8 order is well reproduced by a heuristic equation using the observed projection of the imidazole ring onto the tetrapyrrole plane (~ − 30° angle with the reference NA–NC axis in PDB entry 6CII). In contrast, the ordering in Fe(III) K53R THB1 without added exogenous ligand (8 ~ 5 > 1 > 3) predicts an imidazole orientation approximately perpendicular to the WT orientation. The NMR data show no indication of such a rearrangement, either by rotation of the proximal histidine ring or the heme, and an orbital explanation for the hyperfine shifts that takes into account the distal ligand remains to be elaborated.

To investigate distal ligation further by NMR spectroscopy, K53R THB1 was uniformly labeled with $^{13}C$ and $^{15}N$. A conventional suite of triple resonance experiments was used to achieve nearly complete backbone assignments (Table S2). The annotated $^1H$–$^{15}N$ HSQC spectrum is given in Fig. S16. The $H^{\alpha}$, $H^{\beta1/\beta2}$ signals of His77 are moderately shifted to 6.96, 7.45 and 5.48 ppm, respectively, and relax quickly (Fig. S14). The $C^{\alpha}$ and $C^{\beta}$, at 62.5 and 32.5 ppm, respectively, are also shifted compared to the diamagnetic WT reference (Table S5). These spectral signatures are consistent with proximal histidine coordination. Assignment of Tyr29 $H^{\beta1/\beta2}$ leads to the ring protons through NOEs, the $^1H$ shifts and width giving no indication of proximity to the paramagnetic center. The HBHA(CO)NH spectrum shows that the Arg53 $H^{\beta1/\beta2}$ signals have "normal" shifts (2.55 and 2.11 ppm), but the remaining methylene signals were not observed in the H(CCO)NH TOCSY experiment.

The conspicuous $^1H$ resonating at 41 and 59 ppm have short $^1H$ $T_1$ values (~15 ms) and a $^{13}C$-detect approach was taken to assign the signals. The $^{13}C$-detect insensitive nuclei enhanced by polarization transfer (INEPT) sequence (Fig. S1A) correlates both $^1H$ with a single $^{13}C$ nucleus resonating at −1 ppm (Fig. 9A). To connect this methylene group to other protein signals, a tailored $^{13}C$-detect TOCSY experiment (Fig. S1B) was used. Detection of the $^{13}C$ signal at −1 ppm identifies four additional $^1H$ within the spin system (Fig. 9B). Of these, two are identified above as the Arg53 $H^{\beta1/\beta2}$ signals, and one is correlated with the resolved $H^{\gamma1/\gamma2}$ signal in the $^1H$–$^1H$ DQF-COSY data (not shown). Correlation of $H^{\gamma1/\gamma2}$ with $C^{\gamma}$ then completes assignment of the aliphatic portion of Arg53 (Fig. 9C) and confirms that the 59 and 41 ppm resonances correspond to $H^{\delta1/\delta2}$. The temperature response (Fig. S15) and large hyperfine shifts of these signals demonstrate a role for Arg53 in the iron coordination sphere of K53R THB1. In addition to the carbon-bound protons, an exchangeable signal integrating as one proton is detected at −24 ppm. This signal is tentatively assigned to Arg53 $H^{\varepsilon}$.

In keeping with the bound hydroxide model and the location of Arg53, we hypothesized that stabilization of the hydroxymet complex would involve hydrogen bonding to the guanidinium headgroup. Evidence for such interactions was sought by acquiring NMR spectra in $^1H_2O/^2H_2O$ solvent mixtures. Fig. 9D–F presents the $H^{\delta1/\delta2}$ signals in $^1H_2O$, $^2H_2O$, and an equal (v:v) mixture of $^1H_2O$ and $^2H_2O$. This last spectrum shows the broadening of the 59 ppm signal and a splitting of the 41 ppm signal in two lines of equal intensity and separated by ~100 Hz. Thus, within a small number of bonds of the $C^{\delta}$ methylene, a labile proton is in slow exchange ($k < 100\ s^{-1}$) with bulk solvent. The closest candidate is $N^{\varepsilon}H$ and the data suggest that this group acts as a hydrogen-bond donor to the axial hydroxide [59]. Isotope effects were

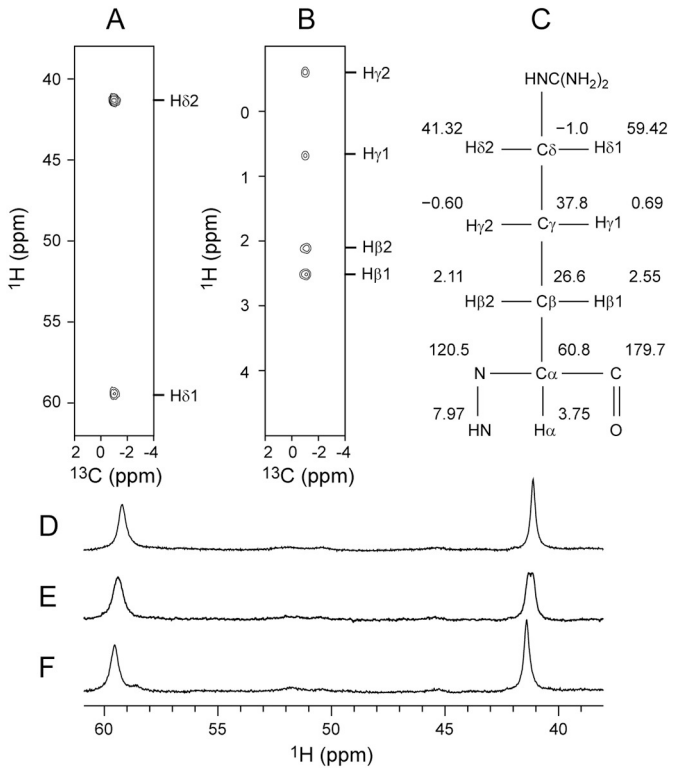


**Fig. 9.** (**A**) The $^{13}C$–$^{1}H$ INEPT spectrum acquired on Fe(III) K53R THB1. Two downfield shifted $^{1}H$ were correlated with a single upfield carbon. (**B**) The tailored H-CC TOCSY spectrum of K53R THB1. Four additional $^{1}H$ were correlated with the upfield $^{13}C$ signal via their attached carbons. Experimental details are provided in Fig. S1. (**C**) Chemical shift assignments for Arg53 in Fe(III) K53R THB1. Stereospecific assignments were made arbitrarily. (**D–F**) Downfield regions of $^{1}H$ NMR spectra of Fe(III) K53R THB1 in different solvent isotope compositions. (**D**) 99% $^{2}H_2O$, pH* 7.9; (**E**) 50% $^{2}H_2O$, pH* 7.9; (**F**) 5% $^{2}H_2O$, pH* 7.5. These spectra were acquired at 25 °C and 600 MHz. Vertical scaling is arbitrary.

also detected on heme signals (resolved methyls and α-vinyl) as expected of a short covalent network connecting Arg53 to the porphyrin substituents.

### 3.4.2. Structural properties of Fe(III) K53R THB1

Chemical shift differences between Fe(III) K53R THB1 and Fe(III) WT THB1 are plotted as CSP in Fig. 8D. The deviations from the WT values extend over the entire sequence except in limited regions of the G and H helices where the distance to the iron exceeds 15 Å and where the structure is disordered (C-terminus). Magnetization transfer to water is detected in the same regions of the protein as in K53H and K53M THB1, i.e., EF loop, disordered termini and the first turn of E helix, suggesting that most CSPs arise from structural distortions rather than fluctuations. Further insight can be gained with an analysis of the $^{13}C$, $^{13}C^{\alpha}$, $^{13}C^{\beta}$, $^{15}N$, and $H^{N}$ chemical shifts using the program TALOS+ [60]. The results are shown in Fig. 10, which also contains the WT information for comparison. The secondary structure is largely maintained with possible alterations in the C and E helices. The EF loop stands out for its lower predicted order parameter in the variant. The WT-based PCS approach described for K53H THB1 failed to provide a reliable tensor. We attribute this to the sensitivity of the PCS to geometry changes and a possible breakdown of the metal-centered point dipole approximation in this complex.

While the position of the residues in Fig. 2 seems to be conserved relative to each other and the heme, strong NOEs between the heme 1-$CH_3$ and Tyr60 and the 8-$CH_3$ and Ala56 in the K53R variant are consistent with the His/Lys THB1 structure. A network of NOEs among

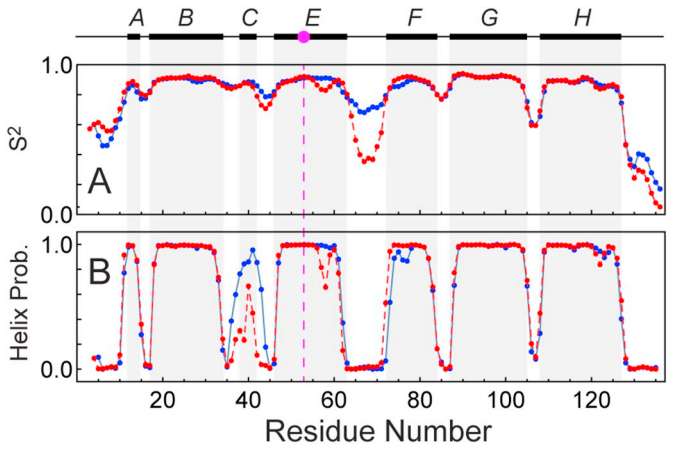


**Fig. 10.** TALOS+ results for Fe(II) WT THB1 (blue) and Fe(III) K53R THB1 (red dashed). (**A**) Predicted order parameter, $S^2$. (**B**) Helical probability. The italicized letters at top denote the helices of the His/Lys THB1 structure (PDB entry 4XDI); the top magenta dot and vertical dashed line indicate the location of residue 53. Helices are represented in the plots as gray bars. (For interpretation of the references to color in this figure legend, the reader is referred to the web version of this article.)

Phe28, Ile32, Phe42 and Val94 also highlights a conserved arrangement of these residues. NOEs between Arg53 $H^{\delta1/\delta2}$ at 41 ppm and Gln54 $H^{\alpha}$, and between the $H^{\delta1/\delta2}$ at 59 ppm and Phe42 $H^{\delta1,\delta2}$ (Fig. S17) orient the aliphatic portion of the Arg53 side chain. The headgroup position remains defined only by the tentative hydrogen bond between $N^{\varepsilon}H$ and the axial hydroxide.

## 4. Discussion

In this work, we initiated the characterization of three new distal variants of THB1 with the goal to inspect the determinants of iron coordination within the group 1 truncated Hb scaffold. We chose residues to complement the WT lysine, one with a higher side chain p$K_a$ (arginine), one with a lower side chain p$K_a$ (histidine), and one not ionizable (methionine). With the reservation that THB1 is one of many examples of the scaffold, but the reassurance that the proteins studied so far are highly structurally related, we can offer some useful observations through comparisons.

### 4.1. Met E10 ligation

The data collected on Fe(II) K53M THB1 confirm that methionine can serve as a heme ligand in the group 1 truncated Hb scaffold. Recent computational and spectroscopic efforts with cytochrome *c* show that the Met–Fe(III) coordination bond is stronger than the Met–Fe(II) bond [61–63]. This is not obvious in Fe(III) K53M THB1 as $H_2O$ outcompetes Met53. Comparison of multiple aligned sequences, grouped according to occupancy at E10, identifies trends in the composition of the E helix immediately prior to E10, specifically a preference for arginines at positions E6, E8, and E9, and leucine at position E7 (Fig. S18). At those positions, THB1 has Lys (E6), Arg (E8) and Arg (E9). As in the majority of group 1 truncated Hbs, position E7 is occupied by a Gln that participates in the H-bond network stabilizing exogenous ligand [41,64]. The presence of Gln E7 in K53M THB1 is expected to favor the binding of $H_2O$ and $OH^-$ in the Fe(III) state, but such bias, which does not operate in the Fe(II) state, would be diminished with Leu E7. It will be interesting to determine if any of the natural sequences that contain Met E10 and Leu E7 adopt the His/Met scheme, whether this scheme occurs in both oxidation states as in cytochrome *c*, and if there is a correlation in the occupancy of the E helix sites mentioned above.

### 4.2. His E10 ligation

Histidine and lysine are the two residues most commonly found at position E10 in group 1 truncated Hbs and, unlike other residues tested in this study, both were found to serve as a distal ligand to Fe(III) and Fe(II) in THB1. Fe(III) K53H THB1 forms a *bis*-histidine complex with no evidence for an aquomet state above pH 4.0, whereas the Fe(II) complex displays a degree of pentacoordinate character at neutral pH. Comparing Fe(II) WT and Fe(II) K53H THB1, similar populations of deligated species are detected at neutral pH. This observation speaks to a preference of THB1 for the native Lys53 ligand over His53 despite the higher intrinsic p$K_a$ of the former residue. Weakened distal histidine coordination to Fe(II) heme, relative to Fe(III), is a feature of *bis*-histidine complexes [65] apparently conserved in K53H THB1. On the other hand, density functional theory calculations of Fe(II) porphine indicate that histidine forms a stronger coordination bond to Fe(II) heme iron than neutral lysine when serving as the sole axial ligand [63]. In the context of THB1, His53 must adjust the structure to form a coordination bond to the iron, and the energetic cost appears to counteract the higher bond strength.

### 4.3. Arg E10 and hydroxide ligation

The most intriguing E10 variant is K53R THB1. To our knowledge, Arg has been documented as a ligand to the heme iron in only one instance, the L130R variant of nitrophorin 4 from *Rhodnius prolixus* in the Fe(II) state (PDB entry 3TGA) [66]. The same complex is not formed in the Fe(III) state in agreement with the hard-soft acid-base concept [67,68]. When modeling Arg53 in the His/Lys structure of THB1 (PDB entry 4XDI), a natural choice of rotamer has *trans* $\chi_1$, $\chi_2$, and $\chi_3$, as Lys53 does. This conformation places the $N^e$ atom at ~2.8 Å from the Fe atom. It is conceivable that direct coordination occurs if $N^e$ is deprotonated and approaches the iron by < 1 Å. Steric clashes between the headgroup and distal cavity residues can readily be avoided by adjusting the last dihedral angle, $\chi_4$, which can adopt a wide range of values in the neutral arginine state. However, the single upfield exchangeable proton in the spectrum of Fe(III) K53R THB1, if correctly assigned to $H^e$, argues against $N^e$ coordination. Alternatively, the dihedral angles could be such as to favor $N^\eta$ coordination. Nevertheless, the His/Arg scheme seems energetically unlikely, especially in the Fe(III) state. In Fe(III) WT THB1, the transition to the aquomet state is half completed at pH ~6.5, whereas half completion is achieved at pH ~6.2 for K53R THB1. The p$K_a$ of a free arginine (13.8, [69]) being much higher than that of a free lysine (10.5, [70]), p$K_{app}$(K53R) would be expected to be measurably higher than p$K_{app}$(WT). Thus, the preferred scheme is His/$OH^-$, stabilized with one or two hydrogen bonds to Arg53, and with $\chi$ angles that extend the side chain and gradually attenuate the hyperfine shift from $C^\delta H_2$ to $C^\alpha H$.

Given the accessibility of a conformation in which residue E10 is expelled toward solvent, it is interesting that Arg53 occupies the distal pocket of K53R THB1. Though a high-resolution structure of K53R THB1 has not been determined yet, NMR structural restraints for residues Arg53 and Tyr60 suggest an orientation of the E helix more similar to the His/Lys structure than the cyanomet conformation of the parent protein. The slow exchange on the chemical shift time scale of the aquomet and hydroxymet states ($k_{ex} < 10^3\ s^{-1}$) is consistent with a concurrent reorganization of the protein requiring the release of Arg–OH hydrogen bonds. Also of note is the population of only one heme orientational isomer, which is unlike what is observed in K53M and K53H THB1 and suggests a restricted steric environment of the heme group.

Arginine residues have functional roles in a number of heme proteins. Arg183 of *Dechloromonas aromatica* chlorite dismutase form hydrogen bonds with substrate and participates in the catalytic decomposition of chlorite to $O_2$ and chloride [71,72]. Horseradish peroxidase uses Arg38 and His42 together to activate $H_2O_2$ and stabilize high-valent intermediates [73,74], and other peroxidases appear to resort to arginine instead of histidine as a catalytic base [75]. Among Hbs, *Aplysia limacina* myoglobin uses an arginine residue in the E helix at the interface between the distal pocket and solvent to stabilize exogenous ligands [76]. The reactivity of K53R THB1 with exogenous ligands has been only briefly investigated at this point. However, addition of $H_2O_2$ causes a gradual bleaching of heme absorbance as in WT THB1 [9] without signatures of a stable oxoferryl intermediate (not shown). Whether Arg E10 fulfills a role other than ligand stabilization in group 1 truncated Hbs is a question for further study.

### 4.4. pH response

The distal variants of THB1 exhibit different responses to pH. This was qualitatively anticipated because of the different intrinsic p$K_a$s and hydrogen bonding capability of the residues involved. However, the apparent p$K_a$ for the aquomet to hydroxymet transition of K53R THB1 (6.2) stands out as particularly low compared to other globins. The Group 2 protein from *Thermobifida fusca* mentioned earlier for its EPR parameters [52] offers a relevant example of low-spin hydroxymet protein. Its apparent p$K_a$ is 7.3, attributed principally to H-bonding with Trp G8, a cavity residue typical of TrHb2s [77]. In K53R THB1, Arg53 would further depress the apparent p$K_a$ with two hydrogen bonds. Also noteworthy is the gap in apparent p$K_a$ for the reduced and oxidized states of K53H THB1, which implies a sizable redox potential difference for the hexa- (His/His) and pentacoordinate (His/−) forms. The physiological significance of these observations will depend on their validity for wild-type proteins rather than artificial variants, but it is clear that THB1 and its relatives are capable of fine-tuning the coordination of the iron with minimal sequence and structure perturbation.

### 4.5. Conformational adaptability in THB1

Axial ligand replacements have been performed in several other proteins with varying consequences. For example, when the distal histidine of neuroglobin, a myoglobin-like globin with wild-type *bis*-histidine ligation, is replaced with a methionine, high spin Fe(III) or Fe(II) complexes are obtained, i.e., no Met coordination occurs [78]. Likewise, Arg replacement in sperm whale myoglobin [79] does not lead to endogenous hexacoordination, whereas the replacement of the distal lysine with histidine in the highly distorted globin fold of the latex clearing protein (Lcp) results in a *bis*-histidine scheme [80]. Replacement of the axial Met100 with lysine in *Thiobacillus versutus* cytochrome $c_{550}$ yields lysine coordination in the Fe(II) state [81] while introduction of Met39 in place of the axial His39 in cytochrome $b_5$ yields Fe(III) His/$H_2O$ and Fe(II) His/Met complexes in analogy with K53M THB1 [82]. The instances that lead to coordination of a non-native residue tend to be associated with its location in flexible loops or secondary structure elements either labile or connected to the rest of the protein with flexible hinges. In all three THB1 variants, the structure of the lysine-bound WT protein is largely preserved. The C and EF hinges, perhaps aided by the fluctuations of the first turn of E helix, appear to control the malleability of the group 1 truncated Hb distal pocket, as proposed on the basis of hydrogen-deuterium exchange and pressure response studies on *Synechococcus* GlbN [83–85]. This plasticity in the distal heme pocket allows TrHbs to adopt variable heme coordination schemes and condition iron reactivity consistent with the demands of the biological context in which they function.

## 5. Conclusions

The group 1 truncated Hb subfamily of proteins can be partitioned according to the residue at the distal position. Replacement of the native distal lysine of THB1 reveals that the protein has a structural scaffold favoring His/Met and His/His states, though with nuances

demonstrated by a range of responses to pH and redox state preferences. The new information can be exploited in the construction of heme proteins with arbitrary properties but also raises the essential question of how to predict endogenous hexacoordination and its chemical consequences across the subfamily. The identification of the structural features subject to reorganization on ligand switching is one step toward the rational control of heme ligation.

## Abbreviations

BLAST Basic Local Alignment Search Tool
BMRB Biological Magnetic Resonance Bank
CSP chemical shift perturbation
DQF-COSY double-quantum-filtered correlated spectroscopy
DT sodium dithionite
Hb hemoglobin
HSQC heteronuclear single-quantum correlation
INEPT insensitive nuclei enhanced by polarization transfer
NOE nuclear Overhauser effect
NOESY nuclear Overhauser spectroscopy
PCS pseudocontact shift
PDB Protein Data Bank
$pH_*$ pH uncorrected for isotope effect
*Synechocystis* GlbN group 1 truncated hemoglobin from *Synechocystis* sp. PCC 6803
*Synechococcus* GlbN group 1 truncated hemoglobin from *Synechococcus* sp. PCC 7002
$T_1$ longitudinal relaxation time
THB1 product of the *THB1* gene, group 1 truncated hemoglobin 1 from *Chlamydomonas reinhardtii*
TOCSY total correlation spectroscopy
TROSY transverse relaxation optimized spectroscopy
WEFT water elimination Fourier transform
WT wild-type

## Declaration of competing interest

None.

## Acknowledgements

The authors thank Dr. Ananya Majumdar for providing the HCC-TOCSY NMR pulse sequence, Dr. Melanie Ehudin in Dr. Kenneth Karlin's laboratory and Dr. Joel Tang for assistance in acquiring EPR data, Dr. Christopher Falzone for feedback and careful reading of the manuscript, Yamini Patibandla for help with protein preparation, and Jaime Martinez and Christos Kougentakis for numerous discussions. All authors declare no competing financial interest.

## Funding

This work was supported by the National Science Foundation grant MCB-1330488 to JTJL and National Institutes of Health grant T32 GM080189 (DBN).

## Appendix A. Supplementary data

Supplementary data to this article can be found online at https://doi.org/10.1016/j.jinorgbio.2019.110824.

## References

[1] T. Li, H.L. Bonkovsky, J.T. Guo, Structural analysis of heme proteins: implications for design and prediction, BMC Struct. Biol. 11 (2011) 13, https://doi.org/10.1186/1472-6807-11-13.
[2] D.A. Landfried, D.A. Vuletich, M.P. Pond, J.T.J. Lecomte, Structural and thermodynamic consequences of *b* heme binding for monomeric apoglobins and other apoproteins, Gene 398 (2007) 12–28, https://doi.org/10.1016/j.gene.2007.02.046.
[3] S. Schneider, J. Marles-Wright, K.H. Sharp, M. Paoli, Diversity and conservation of interactions for binding heme in *b*-type heme proteins, Nat. Prod. Rep. 24 (2007) 621–630, https://doi.org/10.1039/b604186h.
[4] S.N. Vinogradov, L. Moens, Diversity of globin function: enzymatic, transport, storage, and sensing, J. Biol. Chem. 283 (2008) 8773–8777, https://doi.org/10.1074/jbc.R700029200.
[5] S.N. Vinogradov, M. Tinajero-Trejo, R.K. Poole, D. Hoogewijs, Bacterial and archaeal globins — a revised perspective, Biochim. Biophys. Acta 1834 (2013) 1789–1800, https://doi.org/10.1016/j.bbapap.2013.03.021.
[6] M. Couture, T.K. Das, P.Y. Savard, Y. Ouellet, J.B. Wittenberg, B.A. Wittenberg, D.L. Rousseau, M. Guertin, Structural investigations of the hemoglobin of the cyanobacterium *Synechocystis* PCC 6803 reveal a unique distal heme pocket, Eur. J. Biochem. 267 (2000) 4770–4780, https://doi.org/10.1046/j.1432-1327.2000.01531.x.
[7] N.L. Scott, C.J. Falzone, D.A. Vuletich, J. Zhao, D.A. Bryant, J.T.J. Lecomte, Truncated hemoglobin from the cyanobacterium *Synechococcus* sp. PCC 7002: evidence for hexacoordination and covalent adduct formation in the ferric recombinant protein, Biochemistry 41 (2002) 6902–6910, https://doi.org/10.1021/bi025609m.
[8] E.A. Johnson, S.L. Rice, M.R. Preimesberger, D.B. Nye, L. Gilevicius, B.B. Wenke, J.M. Brown, G.B. Witman, J.T.J. Lecomte, Characterization of THB1, a *Chlamydomonas reinhardtii* truncated hemoglobin: linkage to nitrogen metabolism and identification of lysine as the distal heme ligand, Biochemistry 53 (2014) 4573–4589, https://doi.org/10.1021/bi5005206.
[9] E.A. Johnson, M.M. Russo, D.B. Nye, J.L. Schlessman, J.T.J. Lecomte, Lysine as a heme iron ligand: a property common to three truncated hemoglobins from *Chlamydomonas reinhardtii*, Biochim. Biophys. Acta 1862 (2018) 2660–2673, https://doi.org/10.1016/j.bbagen.2018.08.009.
[10] S. Kakar, F.G. Hoffman, J.F. Storz, M. Fabian, M.S. Hargrove, Structure and reactivity of hexacoordinate hemoglobins, Biophys. Chem. 152 (2010) 1–14, https://doi.org/10.1016/j.bpc.2010.08.008.
[11] S.L. Rice, L.E. Boucher, J.L. Schlessman, M.R. Preimesberger, J. Bosch, J.T.J. Lecomte, Structure of *Chlamydomonas reinhardtii* THB1, a group 1 truncated hemoglobin with a rare histidine-lysine heme ligation, Acta Crystallogr. F Struct. Biol. Commun. 71 (2015) 718–725, https://doi.org/10.1107/S2053230X15006949.
[12] E.A. Berry, B.L. Trumpower, Simultaneous determination of hemes *a*, *b*, and *c* from pyridine hemochrome spectra, Anal. Biochem. 161 (1987) 1–15, https://doi.org/10.1016/0003-2697(87)90643-9.
[13] S. Stoll, A. Schweiger, EasySpin, a comprehensive software package for spectral simulation and analysis in EPR, J. Magn. Reson. 178 (2006) 42–55, https://doi.org/10.1016/j.jmr.2005.08.013.
[14] D.S. Wishart, C.G. Bigam, J. Yao, F. Abildgaard, H.J. Dyson, E. Oldfield, J.L. Markley, B.D. Sykes, $^{1}H$, $^{13}C$ and $^{15}N$ chemical shift referencing in biomolecular NMR, J. Biomol. NMR 6 (1995) 135–140, https://doi.org/10.1007/BF00211777.
[15] F. Delaglio, S. Grzesiek, G.W. Vuister, G. Zhu, J. Pfeifer, A. Bax, NMRPipe: a multidimensional spectral processing system based on UNIX pipes, J. Biomol. NMR 6 (1995) 277–293, https://doi.org/10.1007/BF00197809.
[16] T.D. Goddard, D.G. Kneller, SPARKY 3, University of California, San Francisco, 2006.
[17] S. Sun, M. Gill, Y. Li, M. Huang, R.A. Byrd, Efficient and generalized processing of multidimensional NUS NMR data: the NESTA algorithm and comparison of regularization terms, J. Biomol. NMR 62 (2015) 105–117, https://doi.org/10.1007/s10858-015-9923-x.
[18] M.W. Maciejewski, A.D. Schuyler, M.R. Gryk, I.I. Moraru, P.R. Romero, E.L. Ulrich, H.R. Eghbalnia, M. Livny, F. Delaglio, J.C. Hoch, NMRbox: a resource for biomolecular NMR computation, Biophys. J. 112 (2017) 1529–1534, https://doi.org/10.1016/j.bpj.2017.03.011.
[19] H. Mo, J.S. Harwood, D. Yang, C.B. Post, A simple method for NMR $t_1$ noise suppression, J. Magn. Reson. 276 (2017) 43–50, https://doi.org/10.1016/j.jmr.2016.12.014.
[20] S.L. Patt, B.D. Sykes, Water eliminated Fourier-transform NMR-spectroscopy, J. Chem. Phys. 56 (1972) 3182–3184, https://doi.org/10.1063/1.1677669.
[21] A. Bax, S. Grzesiek, Methodological advances in protein NMR, Acc. Chem. Res. 26 (1993) 131–138, https://doi.org/10.1021/ar00028a001.
[22] Y. Lin, G. Wagner, Efficient side-chain and backbone assignment in large proteins: application to tGCN5, J. Biomol. NMR 15 (1999) 227–239, https://doi.org/10.1023/A:1008343915382.
[23] S.G. Hyberts, K. Takeuchi, G. Wagner, Poisson-gap sampling and forward maximum entropy reconstruction for enhancing the resolution and sensitivity of protein NMR data, J. Am. Chem. Soc. 132 (2010) 2145–2147, https://doi.org/10.1021/ja908004w.
[24] J. Cavanagh, W.J. Fairbrother, A.G.I. Palmer, M. Rance, N.J. Skelton, Protein NMR spectroscopy, Principles and Practice, 2nd edition, Academic Press, San Diego, USA, 2006.
[25] E.F. Pettersen, T.D. Goddard, C.C. Huang, G.S. Couch, D.M. Greenblatt, E.C. Meng, T.E. Ferrin, UCSF chimera - a visualization system for exploratory research and analysis, J. Comput. Chem. 25 (2004) 1605–1612, https://doi.org/10.1002/jcc.20084.
[26] S.D. Emerson, G.N. La Mar, NMR determination of the orientation of the magnetic susceptibility tensor of cyano metmyoglobin: a new probe of steric tilt of bound ligand, Biochemistry 29 (1990) 1556–1566, https://doi.org/10.1021/bi00458a029.

[27] R.W. Hendler, R.I. Shrager, Deconvolutions based on singular value decomposition and the pseudoinverse: a guide for beginners, J. Biochem. Biophys. Methods 28 (1994) 1–33, https://doi.org/10.1016/0165-022X(94)90061-2.

[28] S.F. Altschul, T.L. Madden, A.A. Schäffer, J. Zhang, Z. Zhang, W. Miller, D.J. Lipman, Gapped BLAST and PSI-BLAST: a new generation of protein database search programs, Nucleic Acids Res. 25 (1997) 3389–3402, https://doi.org/10.1093/nar/25.17.3389.

[29] A.M. Waterhouse, J.B. Procter, D.M. Martin, M. Clamp, G.J. Barton, Jalview version 2–a multiple sequence alignment editor and analysis workbench, Bioinformatics 25 (2009) 1189–1191, https://doi.org/10.1093/bioinformatics/btp033.

[30] D.B. Nye, J.T.J. Lecomte, Replacement of the distal histidine reveals a noncanonical heme binding site in a 2-on-2 hemoglobin, Biochemistry 57 (2018) 5785–5796, https://doi.org/10.1021/acs.biochem.8b00752.

[31] S.D. Emerson, G.N. La Mar, Solution structural characterization of cyano-metmyoglobin: resonance assignment of heme cavity residues by two-dimensional NMR, Biochemistry 29 (1990) 1545–1555, https://doi.org/10.1021/bi00458a028.

[32] B.C. Vu, H.J. Nothnagel, D.A. Vuletich, C.J. Falzone, J.T.J. Lecomte, Cyanide binding to hexacoordinate cyanobacterial hemoglobins: hydrogen bonding network and heme pocket rearrangement in ferric H117A *Synechocystis* Hb, Biochemistry 43 (2004) 12622–12633, https://doi.org/10.1021/bi048726l.

[33] L.J. Smith, A. Kahraman, J.M. Thornton, Heme proteins–diversity in structural characteristics, function, and folding, Proteins 78 (2010) 2349–2368, https://doi.org/10.1002/prot.22747.

[34] K. Shikama, A. Matsuoka, Spectral properties unique to the myoglobins lacking the usual distal histidine residue, J. Mol. Biol. 209 (1989) 489–491, https://doi.org/10.1016/0022-2836(89)90012-0.

[35] J. McKnight, M.R. Cheesman, A.J. Thomson, J.S. Miles, A.W. Munro, Identification of charge-transfer transitions in the optical spectrum of low-spin ferric cytochrome P-450 *Bacillus megaterium*, Eur. J. Biochem. 213 (1993) 683–687, https://doi.org/10.1111/j.1432-1033.1993.tb17808.x.

[36] W.D. Butt, D. Keilin, Absorption spectra and some other properties of cytochrome *c* and of its compounds with ligands, Proc. R. Soc. Lond. B Biol. Sci. 156 (1962) 429–458, https://doi.org/10.1098/rspb.1962.0049.

[37] G.N. La Mar, N.L. Davis, D.W. Parish, K.M. Smith, Heme orientational disorder in reconstituted and native sperm whale myoglobin. Proton nuclear magnetic resonance characterizations by heme methyl deuterium labeling in the met-cyano protein, J. Mol. Biol. 168 (1983) 887–896, https://doi.org/10.1016/S0022-2836(83)80080-1.

[38] H. Senn, A. Eugster, K. Wüthrich, Determination of the coordination geometry at the heme iron in three cytochromes *c* from *Saccharomyces cerevisiae* and from *Candida krusei* based on individual $^{1}$H-NMR assignments for heme *c* and the axially coordinated amino acids, Biochim. Biophys. Acta 743 (1983) 58–68, https://doi.org/10.1016/0167-4838(83)90418-1.

[39] K.L. Bren, J.A. Kellogg, R. Kaur, X. Wen, Folding, conformational changes, and dynamics of cytochromes *c* probed by NMR spectroscopy, Inorg. Chem. 43 (2004) 7934–7944, https://doi.org/10.1021/ic048925t.

[40] M.W. Mara, R.G. Hadt, M.E. Reinhard, T. Kroll, H. Lim, R.W. Hartsock, R. Alonso-Mori, M. Chollet, J.M. Glownia, S. Nelson, D. Sokaras, K. Kunnus, K.O. Hodgson, B. Hedman, U. Bergmann, K.J. Gaffney, E.I. Solomon, Metalloprotein entatic control of ligand-metal bonds quantified by ultrafast X-ray spectroscopy, Science 356 (2017) 1276–1280, https://doi.org/10.1126/science.aam6203.

[41] A. Pesce, M. Couture, S. Dewilde, M. Guertin, K. Yamauchi, P. Ascenzi, L. Moens, M. Bolognesi, A novel two-over-two α-helical sandwich fold is characteristic of the truncated hemoglobin family, EMBO J. 19 (2000) 2424–2434, https://doi.org/10.1093/emboj/19.11.2424.

[42] O. Einsle, A. Messerschmidt, R. Huber, P.M.H. Kroneck, F. Neese, Mechanism of the six-electron reduction of nitrite to ammonia by cytochrome *c* nitrite reductase, J. Am. Chem. Soc. 124 (2002) 11737–11745, https://doi.org/10.1021/ja0206487.

[43] R.E. Berry, X.D. Ding, T. Shokhireva, A. Weichsel, W.R. Montfort, F.A. Walker, Axial ligand complexes of the *Rhodnius* nitrophorins: reduction potentials, binding constants, EPR spectra, and structures of the 4-iodopyrazole and imidazole complexes of NP4, J. Biol. Inorg. Chem. 9 (2004) 135–144, https://doi.org/10.1007/s00775-003-0505-0.

[44] N. Kunishima, F. Amada, K. Fukuyama, M. Kawamoto, T. Matsunaga, H. Matsubara, Pentacoordination of the heme iron of *Arthromyces ramosus* peroxidase shown by a 1.8 Å resolution crystallographic study at pH 4.5, FEBS Lett. 378 (1996) 291–294, https://doi.org/10.1016/0014-5793(95)01458-6.

[45] F.A. Walker, B.H. Huynh, W.R. Scheidt, S.R. Osvath, Models of the cytochromes *b*. Effect of axial ligand plane orientation on the EPR and Moessbauer spectra of low-spin ferrihemes, J. Am. Chem. Soc. 108 (1986) 5288–5297, https://doi.org/10.1021/ja00277a038.

[46] F.A. Walker, Magnetic spectroscopic (EPR, ESEEM, Mössbauer, MCD and NMR) studies of low-spin ferriheme centers and their corresponding heme proteins, Coord. Chem. Rev. 185-186 (1999) 471–534, https://doi.org/10.1016/S0010-8545(99)00029-6.

[47] G.N. La Mar, J.D. Satterlee, J.S. de Ropp, Nuclear magnetic resonance of hemoproteins, in: K.M. Smith, K. Kadish, R. Guilard (Eds.), The Porphyrin Handbook, vol. 5, Academic Press, Burlington, MA, 2000, pp. 185–298.

[48] N.V. Shokhirev, F.A. Walker, The effect of axial ligand plane orientation on the contact and pseudocontact shifts of low-spin ferriheme proteins, J. Biol. Inorg. Chem. 3 (1998) 581–594, https://doi.org/10.1007/s007750050271.

[49] J.A. Hoy, S. Kundu, J.T. Trent 3rd, S. Ramaswamy, M.S. Hargrove, The crystal structure of *Synechocystis* hemoglobin with a covalent heme linkage, J. Biol. Chem. 279 (2004) 16535–16542, https://doi.org/10.1074/jbc.M313707200.

[50] B.B. Wenke, J.T.J. Lecomte, A. Héroux, J.L. Schlessman, The 2/2 hemoglobin from the cyanobacterium *Synechococcus* sp. PCC 7002 with covalently attached heme: comparison of X-ray and NMR structures, Proteins 82 (2014) 528–534, https://doi.org/10.1002/prot.24409.

[51] W.E. Blumberg, J. Peisach, A unified theory for low spin forms of all ferric heme proteins as studied by EPR, in: B. Chance, T. Yonetani, A.S. Mildvan (Eds.), Probes of Structure and Function of Macromolecules and Membranes, II Academic Press, New York, 1971, pp. 215–227.

[52] F.P. Nicoletti, J.P. Bustamante, E. Droghetti, B.D. Howes, M. Fittipaldi, A. Bonamore, P. Baiocco, A. Feis, A. Boffi, D.A. Estrin, G. Smulevich, Interplay of the H-bond donor–acceptor role of the distal residues in hydroxyl ligand stabilization of *Thermobifida fusca* truncated hemoglobin, Biochemistry 53 (2014) 8021–8030, https://doi.org/10.1021/bi501132a.

[53] K.D. Egeberg, B.A. Springer, S.A. Martinis, S.G. Sligar, D. Morikis, P.M. Champion, Alteration of sperm whale myoglobin heme axial ligation by site-directed mutagenesis, Biochemistry 29 (1990) 9783–9791, https://doi.org/10.1021/bi00494a004.

[54] K. Nagai, T. Kagimoto, A. Hayashi, F. Taketa, T. Kitagawa, Resonance raman studies of hemoglobins M: evidence for iron-tyrosine charge-transfer interactions in the abnormal subunits of Hb M Boston and Hb M Iwate, Biochemistry 22 (1983) 1305–1311, https://doi.org/10.1021/bi00274a048.

[55] G.G. Silkstone, C.E. Cooper, D. Svistunenko, M.T. Wilson, EPR and optical spectroscopic studies of Met80X mutants of yeast ferricytochrome *c*. Models for intermediates in the alkaline transition, J. Am. Chem. Soc. 127 (2005) 92–99, https://doi.org/10.1021/ja045719b.

[56] C. Caillet-Saguy, M. Delepierre, A. Lecroisey, I. Bertini, M. Piccioli, P. Turano, Direct-detected $^{13}$C NMR to investigate the iron(III) hemophore HasA, J. Am. Chem. Soc. 128 (2006) 150–158, https://doi.org/10.1021/ja054902h.

[57] L. Banci, I. Bertini, K.L. Bren, H.B. Gray, P. Turano, pH-dependent equilibria of yeast Met80Ala-iso-1-cytochrome *c* probed by NMR spectroscopy: a comparison with the wild-type protein, Chem. Biol. 2 (1995) 377–383, https://doi.org/10.1016/1074-5521(95)90218-X.

[58] I. Bertini, C. Luchinat, G. Parigi, F.A. Walker, Heme methyl $^{1}$H chemical shifts as structural parameters in some low-spin ferriheme proteins, J. Biol. Inorg. Chem. 4 (1999) 515–519, https://doi.org/10.1007/s007750050337.

[59] B. Xia, S.J. Wilkens, W.M. Westler, J.L. Markley, Amplification of one-bond $^{1}$H/$^{2}$H isotope effects on $^{15}$N chemical shifts in *Clostridium pasteurianum* rubredoxin by Fermi-contact effects through hydrogen bonds, J. Am. Chem. Soc. 120 (1998) 4893–4894, https://doi.org/10.1021/ja974167c.

[60] Y. Shen, F. Delaglio, G. Cornilescu, A. Bax, TALOS+: a hybrid method for predicting protein backbone torsion angles from NMR chemical shifts, J. Biomol. NMR 44 (2009) 213–223, https://doi.org/10.1007/s10858-009-9333-z.

[61] T. Kroll, R.G. Hadt, S.A. Wilson, M. Lundberg, J.J. Yan, T.C. Weng, D. Sokaras, R. Alonso-Mori, D. Casa, M.H. Upton, B. Hedman, K.O. Hodgson, E.I. Solomon, Resonant inelastic X-ray scattering on ferrous and ferric bis-imidazole porphyrin and cytochrome *c*: nature and role of the axial methionine-Fe bond, J. Am. Chem. Soc. 136 (2014) 18087–18099, https://doi.org/10.1021/ja5100367.

[62] T. Wondimagegn, A. Rauk, The structures and stabilities of the complexes of biologically available ligands with Fe(III)-porphine: an ab initio study, J. Phys. Chem. B 115 (2011) 569–579, https://doi.org/10.1021/jp1090747.

[63] T. Wondimagegn, A. Rauk, The structures and stabilities of the complexes of biologically available ligands with Fe(II) porphine: an ab initio study, J. Phys. Chem. B 116 (2012) 10301–10310, https://doi.org/10.1021/jp305864y.

[64] J. Igarashi, K. Kobayashi, A. Matsuoka, A hydrogen-bonding network formed by the B10-E7-E11 residues of a truncated hemoglobin from *Tetrahymena pyriformis* is critical for stability of bound oxygen and nitric oxide detoxification, J. Biol. Inorg. Chem. 16 (2011) 599–609, https://doi.org/10.1007/s00775-011-0761-3.

[65] A.B. Cowley, A. Altuve, O. Kuchment, S. Terzyan, X. Zhang, M. Rivera, D.R. Benson, Toward engineering the stability and hemin-binding properties of microsomal cytochromes $b_5$ into rat outer mitochondrial membrane cytochrome $b_5$: examining the influence of residues 25 and 71, Biochemistry 41 (2002) 11566–11581, https://doi.org/10.1021/bi026005l.

[66] C. He, M.R. Fuchs, H. Ogata, M. Knipp, Guanidine-ferroheme coordination in the mutant protein nitrophorin 4(L130R), Angew. Chem. Int. Ed. Engl. 51 (2012) 4470–4473, https://doi.org/10.1002/anie.201108691.

[67] J. Stanek, T. Rösener, A. Metz, J. Mannsperger, A. Hoffmann, S. Herres-Pawlis, Guanidine metal complexes for bioinorganic chemistry and polymerisation catalysis, in: P. Selig (Ed.), Guanidines as Reagents and Catalysts II, Springer International Publishing, Cham, 2017, pp. 95–164, , https://doi.org/10.1007/7081_2015_173.

[68] A.J. Bhattacharyya, M.P. Schmidt, E. Stavitski, B. Azimzadeh, C.E. Martínez, Ligands representing important functional groups of natural organic matter facilitate Fe redox transformations and resulting binding environments, Geochim. Cosmochim. Acta 251 (2019) 157–175, https://doi.org/10.1016/j.gca.2019.02.027.

[69] C.A. Fitch, G. Platzer, M. Okon, B. Garcia-Moreno E, L.P. McIntosh, Arginine: its p$K_a$ value revisited, Protein Sci. 24 (2015) 752–761, https://doi.org/10.1002/pro.2647.

[70] G.R. Grimsley, J.M. Scholtz, C.N. Pace, A summary of the measured p*K* values of the ionizable groups in folded proteins, Protein Sci. 18 (2009) 247–251, https://doi.org/10.1002/pro.19.

[71] B. Blanc, J.A. Mayfield, C.A. McDonald, G.S. Lukat-Rodgers, K.R. Rodgers, J.L. DuBois, Understanding how the distal environment directs reactivity in chlorite dismutase: spectroscopy and reactivity of Arg183 mutants, Biochemistry 51 (2012) 1895–1910, https://doi.org/10.1021/bi2017377.

[72] B.R. Streit, B. Blanc, G.S. Lukat-Rodgers, K.R. Rodgers, J.L. DuBois, How active-site protonation state influences the reactivity and ligation of the heme in chlorite dismutase, J. Am. Chem. Soc. 132 (2010) 5711–5724, https://doi.org/10.1021/ja9082182.

[73] J.N. Rodriguez-Lopez, A.T. Smith, R.N. Thorneley, Role of arginine 38 in horseradish peroxidase. A critical residue for substrate binding and catalysis, J. Biol. Chem. 271 (1996) 4023–4030, https://doi.org/10.1074/jbc.271.8.4023.
[74] S. Tatoli, C. Zazza, N. Sanna, A. Palma, M. Aschi, The role of arginine 38 in horseradish peroxidase enzyme revisited: a computational investigation, Biophys. Chem. 141 (2009) 87–93, https://doi.org/10.1016/j.bpc.2008.12.015.
[75] R. Singh, J.C. Grigg, Z. Armstrong, M.E. Murphy, L.D. Eltis, Distal heme pocket residues of B-type dye-decolorizing peroxidase: arginine but not aspartate is essential for peroxidase activity, J. Biol. Chem. 287 (2012) 10623–10630, https://doi.org/10.1074/jbc.M111.332171.
[76] E. Conti, C. Moser, M. Rizzi, A. Mattevi, C. Lionetti, A. Coda, P. Ascenzi, M. Brunori, M. Bolognesi, X-ray crystal structure of ferric *Aplysia limacina* myoglobin in different liganded states, J. Mol. Biol. 233 (1993) 498–508, https://doi.org/10.1006/jmbi.1993.1527.
[77] D.A. Vuletich, J.T.J. Lecomte, A phylogenetic and structural analysis of truncated hemoglobins, J. Mol. Evol. 62 (2006) 196–210, https://doi.org/10.1007/s00239-005-0077-4.
[78] H.X. Liu, L. Li, B. He, S.Q. Gao, G.B. Wen, Y.W. Lin, Neuroglobin is capable of self-oxidation of methionine64 introduced at the heme axial position, Dalton Trans. 47 (2018) 10847–10852, https://doi.org/10.1039/c8dt02397b.
[79] C.T. Allocatelli, F. Cutruzzola, A. Brancaccio, M. Brunori, J. Qin, G.N. La Mar, Structural and functional characterization of sperm whale myoglobin mutants: role of arginine (E10) in ligand stabilization, Biochemistry 32 (1993) 6041–6049, https://doi.org/10.1021/bi00074a015.
[80] L. Ilcu, W. Rother, J. Birke, A. Brausemann, O. Einsle, D. Jendrossek, Structural and functional analysis of latex clearing protein (Lcp) provides insight into the enzymatic cleavage of rubber, Sci. Rep. 7 (2017) 6179, https://doi.org/10.1038/s41598-017-05268-2.
[81] M. Ubbink, A.P. Campos, M. Teixeira, N.I. Hunt, H.A. Hill, G.W. Canters, Characterization of mutant Met100Lys of cytochrome *c*-550 from *Thiobacillus versutus* with lysine-histidine heme ligation, Biochemistry 33 (1994) 10051–10059, https://doi.org/10.1021/bi00199a032.
[82] S.G. Sligar, K.D. Egeberg, J.T. Sage, D. Morikis, P.M. Champion, Alteration of heme axial ligands by site-directed mutagenesis: a cytochrome becomes a catalytic demethylase, J. Am. Chem. Soc. 109 (1987) 7896–7897, https://doi.org/10.1021/ja00259a056.
[83] M.P. Pond, A. Majumdar, J.T.J. Lecomte, Influence of heme post-translational modification and distal ligation on the backbone dynamics of a monomeric hemoglobin, Biochemistry 51 (2012) 5733–5747, https://doi.org/10.1021/bi300624a.
[84] D.A. Vuletich, C.J. Falzone, J.T.J. Lecomte, Structural and dynamic repercussions of heme binding and heme-protein cross-linking in *Synechococcus* sp. PCC 7002 hemoglobin, Biochemistry 45 (2006) 14075–14084, https://doi.org/10.1021/bi061532g.
[85] M. Dellarole, C. Roumestand, C. Royer, J.T.J. Lecomte, Volumetric properties underlying ligand binding in a monomeric hemoglobin: a high-pressure NMR study, Biochim. Biophys. Acta 1834 (2013) 1910–1922, https://doi.org/10.1016/j.bbapap.2013.04.016.